RESEARCH ARTICLE

Key Points:
- Modeling the ρ and V_Φ profiles of the lower mantle using self-consistent pressure scales and new constraints on Ca-Pv
- Comparing with PREM, a pyrolitic mantle is preferred over a chondritic mantle
- The amount of Ca-Pv cannot be constrained based on the density and bulk sound velocity profiles as its elasticity lies close to PREM

Confirming a pyrolitic lower mantle using self-consistent pressure scales and new constraints on CaSiO₃ perovskite

Ningyu Sun[1], Zhu Mao[1,2], Shuai Yan[1], Xiang Wu[3], Vitali B. Prakapenka[4], and Jung-Fu Lin[5,6]

[1]Laboratory of Seismology and Physics of Earth's Interior, School of Earth and Planetary Sciences, University of Science and Technology of China, Hefei, China, [2]National Geophysics Observatory, Mengcheng, China, [3]State Key Laboratory of Geological Processes and Mineral Resources, China University of Geosciences, Wuhan, China, [4]Center for Advanced Radiation Sources, University of Chicago, Chicago, Illinois, USA, [5]Department of Geological Sciences, Jackson School of Geosciences, University of Texas at Austin, Austin, Texas, USA, [6]Center for High Pressure Science and Technology Advanced Research, Shanghai, China

Abstract In this study, we have examined the lower mantle composition and mineralogy by modeling the density (ρ), bulk sound velocity (V_Φ), and $d\ln\rho/d\ln V_\Phi$ profiles of candidate lower mantle minerals using literature and new experimental equation of state (EoS) results. For CaSiO₃ perovskite, complimentary synchrotron X-ray diffraction measurements in a laser-heated diamond anvil cell were conducted up to 156 GPa between 1200 K and 2600 K to provide more reliable constraints on the thermal EoS parameters. These new experimental results as well as literature P-V-T data sets are systematically analyzed using an internally self-consistent pressure scale. We have modeled ρ, V_Φ, and $d\ln\rho/d\ln V_\Phi$ profiles of the lower mantle with representative pyrolitic and chondritic compositional models in which the effect of Fe spin transition in ferropericlase is also taken into account. Our modeling results show that a pyrolitic lower mantle with an aggregate mineralogy of 75 vol % bridgmanite, 17 vol % ferropericlase, and 8 vol % CaSiO₃ perovskite produces ρ and V_Φ profiles in better agreement with preliminary reference Earth model than a lower mantle with a chondritic composition. The modeled ρ, V_Φ, and $d\ln\rho/d\ln V_\Phi$ are mainly affected by the relative ratio of bridgmanite and ferropericlase but are not sensitive to the variation of the CaSiO₃ perovskite content. In addition, the spin crossover of Fe in ferropericlase can greatly raise the value of $d\ln\rho/d\ln V_\Phi$ in the middle lower mantle, which is useful in detecting the presence of ferropericlase in the region. Based on these new mineral physical constraints and radial seismic structure, our study suggests the lower mantle is pyrolitic, which is chemically indistinguishable from the upper mantle.

1. Introduction

Knowledge of the lower mantle mineralogy and composition is essential for understanding the formation, differentiation, and dynamic evolution of the Earth [e.g., *Hofmann*, 1988; *Kaminski and Javoy*, 2013; *Lee et al.*, 2010; *Mcdonough and Sun*, 1995]. Although chemical composition of the Earth's lower mantle is a fundamental question for geophysical and geochemical studies, it has long been a debated topic due to limited samples available and direct experimental support [e.g., *Anderson*, 1983; *Javoy*, 1995; *Mcdonough and Sun*, 1995; *Morgan and Anders*, 1980; *Palme and Jones*, 2003; *Ringwood*, 1975]. Numerous attempts have been made to constrain the lower mantle composition using seismic observations, laboratory and theoretical mineral physics results, analysis of terrestrial samples, and cosmochemical data. One key difference between previously proposed geochemical and cosmochemical models of the mantle is that the Mg/Si ratio varies from approximately 1 in the chondritic composition model to 1.3 in the pyrolitic model [e.g., *Anderson*, 1983; *Hart and Zindler*, 1986; *Javoy*, 1995; *Ringwood*, 1975]. Petrological evidence obtained from the compositional trends in upper mantle peridotites suggests that the Mg/Si ratio of the bulk silicate Earth is close to 1.27, indicating a homogeneous upper and lower mantle in composition [*Anderson*, 1983; *Ringwood*, 1975]. In the pyrolitic compositional model of the mantle, so-called the pyrolite model, the lower mantle is consisted of 75 vol % bridgmanite [(Mg,Fe)(Al,Si)O₃], 17 vol % ferropericlase [(Mg,Fe)O], and 8 vol % CaSiO₃ perovskite [*Ringwood*, 1975]. However, if the terrestrial planets, meteorites, and the sun were accreted from similar materials in the solar nebula, the composition of the Earth could be represented by chondritic meteorites [e.g., *Javoy*, 1995; *Mcdonough and Sun*, 1995; *Morgan and Anders*, 1980; *Williams and Knittle*, 2005]. If the mantle has a composition of CI chondrites, the Mg/Si ratio was estimated to be 1.074, which would suggest a

compositional distinct upper and lower mantle [*Hart and Zindler*, 1986]. Lower mantle with a chondritic compositional model thus needs to be enriched in bridgmanite and Ca-perovskite with a Mg/Si ratio of ~1 [*Anderson*, 1989].

Comparison of the laboratory measurements for the density and velocity of candidate lower mantle minerals with seismic observations provides one of the most established means to infer the mineralogy and chemical composition of the planet's deep region [e.g., *Cammarano and Romanowicz*, 2007; *Duffy and Anderson*, 1989; *Li and Liebermann*, 2007; *Mao et al.*, 2014; *Matas et al.*, 2007]. However, direct experimental measurements on the elasticity and sound velocity of lower mantle minerals at relevant pressure and temperature (P-T) conditions of the lower mantle are significantly limited. Thus far, only shear-wave velocities of lower mantle bridgmanite and ferropericlase were measured at simultaneously high P-T conditions relevant to the lower mantle, indicating that a Si-enriched lower mantle with more than 93% bridgmanite will have a shear-wave velocity profile in better agreement with the seismic preliminary reference Earth model (PREM) than lower mantle with a pyrolitic composition [*Dziewonski and Anderson*, 1981; *Murakami et al.*, 2012]. However, the velocity models in *Murakami et al.* [2012] did not consider the contribution of CaSiO$_3$ perovskite, the third most abundant phase in the lower mantle, and did not examine whether the density of a Si-enriched lower mantle can also match well with PREM as well as the velocity profiles. Furthermore, a recent study pointed out that incorrectly averaging the velocities of a multiple-component system may lead to the conclusion of a highly bridgmanite-enriched lower mantle [*Cottaar et al.*, 2014]. Extensive theoretical and modeling efforts have been made to understand the composition of the region. For example, the effect of composition variation on the velocity of the lower mantle was examined by using literature elastic parameters of candidate minerals which were determined either by experimental or theoretical studies [*Matas et al.*, 2007]. It shows that the best velocity model in order to reasonably fit the 1-D seismic profiles requires the Mg/Si ratio in the lower mantle to be less than that in a pyrolitic mantle composition [*Matas et al.*, 2007]. It should be noted that the Mg/Si ratio in the lower mantle suggested by *Matas et al.* [2007] exhibits a strong dependence on the value for the pressure derivative of the shear modulus (dG/dP) of bridgmanite and the temperature gradient in the lower mantle. The pressure derivative of the shear modulus of bridgmanite has not been constrained by simultaneous high P-T experimental studies when *Matas et al.* [2007] performed the analysis, which could affect the estimated lower mantle composition. In contrast to recent experimental results [*Murakami et al.*, 2012], theoretical studies using first-principle methods to model the density and velocities of the lower mantle in various compositions conclude that lower mantle in a pyrolitic composition has density and velocity profiles matching the seismic PREM better [*Wang et al.*, 2015; *Zhang et al.*, 2016].

Due to limited experimental constraints on the elasticity and sound velocity of lower mantle minerals at P-T conditions relevant to the lower mantle, an alternative way to estimate and constrain the lower mantle composition is to compare the density (ρ) and bulk sound velocity (V_Φ) profiles of candidate lower mantle minerals with a 1-D seismic model. In the past 20 years, tremendous effort has been made to determine the pressure-volume-temperature (P-V-T) and thus the thermal equation of state (EoS) parameters of minerals at relevant P-T conditions of the lower mantle [e.g., *Fiquet et al.*, 2000; *Komabayashi et al.*, 2010; *Mao et al.*, 2011a; *Shim et al.*, 2000; *Speziale et al.*, 2001; *Tange et al.*, 2012]. Evaluation of the P-V-T relations of candidate mantle minerals also provides some constraints on the ratios of seismic heterogeneities via the ratio of density to bulk sound velocity (dlnρ/dlnV_Φ). One major problem to build reliable ρ and V_Φ profiles using thermal EoS parameters in literature is the use of different pressure scales and calibrants, such as Au, Pt, and ruby in previous experiments, which can result in great difficulties when comparing the obtained thermal EoS parameters between different studies [e.g., *Ballaran et al.*, 2012; *Fiquet et al.*, 2000; *Jacobsen et al.*, 2008; *Komabayashi et al.*, 2010; *Lundin et al.*, 2008; *Mao et al.*, 2011b]. Since the absolute pressure scale of a pressure calibrant remains to be firmly established, a reliable, self-consistent pressure scale at relevant P-T conditions of the lower mantle should be used to reevaluate the literature pressure-volume (P-V) data in order to better constrain the thermal EoS parameters of the lower mantle minerals.

Other than the aforementioned high P-T effects on the EoS parameters, the effect of spin transition needs to be considered. Recent high P-T experimental studies show that Fe in lower mantle bridgmanite and ferropericlase will undergo the spin transition [e.g., *Badro et al.*, 2003; *Li et al.*, 2004; *Lin et al.*, 2013]. The spin transition of Fe can produce an anomalous increase in ρ and a softening in V_Φ of ferropericlase at relevant P-T conditions of the lower mantle [e.g., *Chen et al.*, 2012; *Komabayashi et al.*, 2010; *Lin et al.*, 2005, 2013; *Mao et al.*, 2011a; *Wentzcovitch et al.*, 2009; *Yang et al.*, 2015]. For lower mantle bridgmanite, recent experimental and theoretical studies are in general agreement that Fe^{2+} in the large pseudododecahedral sites
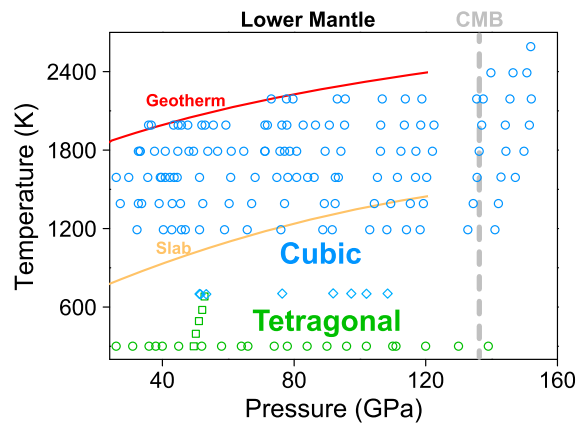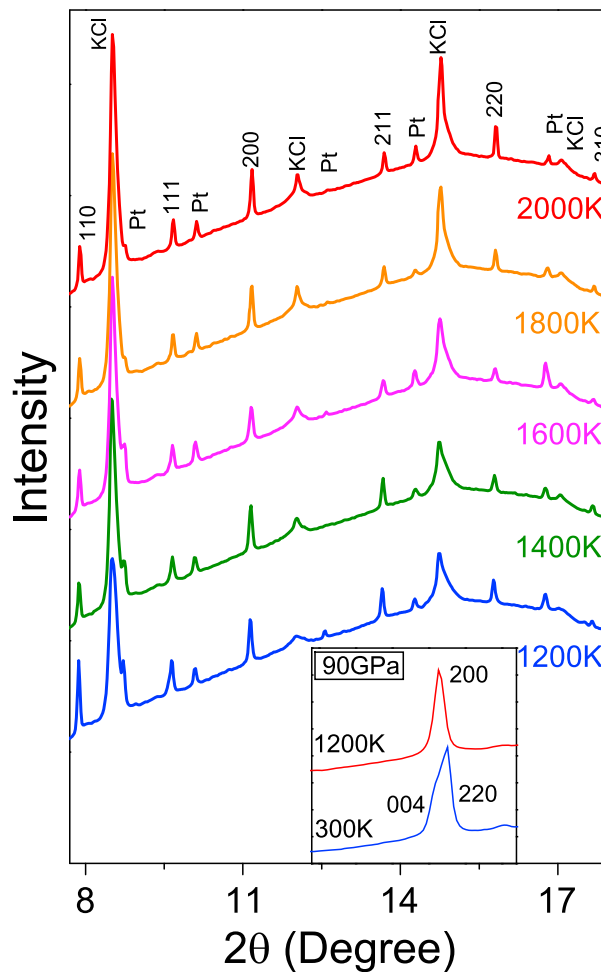
Figure 1. Experimental P-T conditions of $CaSiO_3$ perovskite. Blue symbols: cubic $CaSiO_3$ perovskite; green symbols: tetragonal $CaSiO_3$ perovskite; circles: this study; diamonds: *Noguchi et al.* [2013]; squares: *Kurashina et al.* [2004]; red line: a typical lower mantle geotherm [*Brown and Shankland*, 1981]; and yellow line: a representative geotherm for the subduction slab [*Kirby et al.*, 1996].

(A site) will exhibit an enhanced lattice distortion at lower mantle pressures, which does not cause an apparent change in the EoS parameters of bridgmanite [*Lin et al.*, 2012; *McCammon et al.*, 2008; *Narygina et al.*, 2010; Mao et al., Equation of state and crystal chemistry of single-crystal bridgmanite in Earth's lower mantle, submitted, 2016]. Although Fe^{3+} in the small octahedral sites (B site) will undergo the high-spin (HS) to low-spin (LS) transition, which has been reported to influence the density of bridgmanite, the amount of B site Fe^{3+} could be greatly limited by the presence of Al in the B site [e.g., *Catalli et al.*, 2010, 2011; *Hsu et al.*, 2011, 2012;

Mao et al., 2015; *Tsuchiya and Wang*, 2013]. Even if one ignores the effect of the Fe spin transition on the ρ and V_Φ profiles of lower mantle bridgmanite, the consequences of the Fe spin transition in ferropericlase on the ρ and V_Φ profiles of the aggregate lower mantle have yet to be examined consistently using the same pressure scale and thermal EoS model, which may result in great uncertainties when estimating the composition of the lower mantle by comparing modeling results with the 1-D seismic profiles [*Matas et al.*, 2007; *Murakami et al.*, 2012]. Thermal EoS modeling incorporating recent mineral physics findings of the Fe spin transition in ferropericlase is thus needed to better constrain the composition of the lower mantle.

Compared to the abundance of bridgmanite and ferropericlase in the lower mantle, $CaSiO_3$ perovskite is a minor phase. However, the volume percentage of $CaSiO_3$ perovskite in the subducted mid-oceanic ridge basalt could be as high as 22–29% [e.g., *Funamori et al.*, 2000; *Hirose et al.*, 1999; *Perrillat et al.*, 2006]. The presence of $CaSiO_3$ perovskite will lower the Mg/Si ratio of the lower mantle and thus influence the mineralogy of the region. $CaSiO_3$ perovskite was found to crystallize in the cubic structure at lower mantle P-T conditions, yet the cubic $CaSiO_3$ perovskite is not temperature quenchable at high pressures; upon temperature quenching, it will transform to the tetragonal structure at high pressures [*Caracas and Wentzcovitch*, 2006; *Jung and Oganov*, 2005; *Ono et al.*, 2004; *Panero et al.*, 2006; *Stixrude et al.*, 2007; *Tamai and Yagi*, 1989]. Recent theoretical study has pointed out that cubic $CaSiO_3$ perovskite in the lower mantle would exhibit a lower shear velocity than that of PREM and a stronger seismic anisotropy than bridgmanite [*Kawai and Tsuchiya*, 2015]. Knowledge on the EoS and elasticity parameters of the cubic $CaSiO_3$ perovskite at high P-T may help explain seismic and geochemical models of the lower mantle. A survey of previous experimental and theoretical studies reveals inconsistent results on the thermoelastic parameters of the cubic $CaSiO_3$ perovskite [*Caracas and Wentzcovitch*, 2006; *Chizmeshya et al.*, 1996; *Hama and Suito*, 1998; *Karki and Crain*, 1998; *Magyari-Kope et al.*, 2002; *Noguchi et al.*, 2013; *Ricolleau et al.*, 2009; *Sherman*, 1993; *Shim et al.*, 2000; *Wang et al.*, 1996; *Wentzcovitch et al.*, 1995; *Wolf and Jeanloz*, 1985; *Zhang et al.*, 2006]. The value of the bulk modulus of the cubic $CaSiO_3$ perovskite at ambient conditions ranges from 216 GPa to 300 GPa in previous studies, leading to significant uncertainties when modeling the density and velocity profiles of the $CaSiO_3$ perovskite in the lower mantle. Other thermoelastic parameters such as the Debye temperature and Grüneisen parameter at ambient conditions in these experimental studies are quite different from theoretical results, potentially due to limited experimental data points, narrow P-T ranges, and/or the use of different pressure calibrants and scales [*Kawai and Tsuchiya*, 2014; *Noguchi et al.*, 2013; *Ricolleau et al.*, 2009; *Shim et al.*, 2000; *Wang et al.*, 1996; *Zhang et al.*, 2006].

The aim of this study is to examine and constrain the composition of the lower mantle by comparison of the modeled ρ and V_Φ profiles of the candidate minerals with the 1-D seismic model. To facilitate this goal, we firstly performed synchrotron X-ray diffraction (XRD) measurements on the P-V-T relation of $CaSiO_3$ perovskite in laser-heated diamond anvil cells (DACs) at temperatures from 1200 K to 2600 K and pressures up to

Figure 2. Representative XRD patterns of CaSiO$_3$ perovskite at high P-T conditions. Cubic CaSiO$_3$ perovskite are labeled with Miller indices (hkl). The incident wavelength, λ, is 0.3344 Å. The insert figure shows the XRD pattern of cubic CaSiO$_3$ perovskite at 1200 K compared with the temperature quenched pattern for tetragonal CaSiO$_3$ perovskite at 300 K at 90 GPa.

156 GPa and discussed the potential cause for the difference in the thermal EoS parameters of the cubic CaSiO$_3$ perovskite in literature. We have also evaluated literature results for the thermal EoS parameters of both bridgmanite and ferropericlase. To avoid the long-standing pressure-scale problem, all the literature P-V data were reanalyzed by recalculating the pressures in literature using a self-consistent pressure scale of *Fei et al.* [2007a]. The new thermal EoS parameters obtained for bridgmanite and ferropericlase can be directly compared between different studies in order to derive the effect of composition on the thermal EoS parameters of relevant minerals. Using the aforementioned thermal EoS parameters of lower mantle minerals, while considering the effect of spin transition on the EoS parameters of ferropericlase and bridgmanite, we have constructed new ρ and V_Φ profiles of the lower mantle for both pyrolitic and chondritic composition models. Comparing our modeled results with the seismic PREM allows us to provide a more comprehensive understanding of the lower mantle seismic profiles and compositional model.

2. Experimental Details

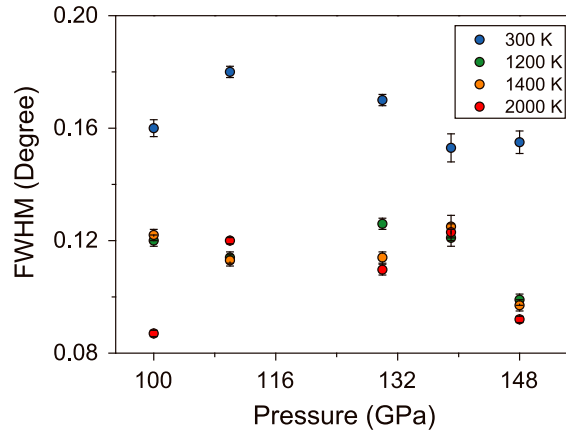Polycrystalline CaSiO$_3$ with purity of 99% was purchased from Sigma-Aldrich Co. LLC. It was ground into a fine powder and used as the starting material. A pressure standard and laser heating absorber of 5 wt % of Pt was mixed with the CaSiO$_3$ powder [*Fei et al.*, 2007a]. The sample mixture was pressed between a pair of diamond anvils to 10–15 μm thick disks which were then cut into pieces of 30–60 μm in diameter. For experiments below 90 GPa, a piece of the sample measuring 60 μm in diameter and 15 μm in thickness was loaded into a symmetric DAC equipped with a pair of diamonds of 200 μm in culet size and a Re gasket with a preindented thickness of 25 μm and a 100 μm drilled hole in the center. We have also prepared two DACs for measurements up to 156 GPa. One DAC was equipped with a pair of beveled diamonds of 150/300 μm in culet size, while the other one has beveled diamonds of 100/300 μm in culet size. The sample pieces were sandwiched between two ~5 μm thick NaCl foils for DAC with 200 μm culet diamonds and KCl foils for DAC with 150/300 μm culet diamonds which were used as the pressure medium and thermal insulator.

The XRD measurements were performed at GeoSoilEnviroConsortium for Advanced Radiation Sources (GSECARS) of the Advanced Photon Source (APS), Argonne National Laboratory (ANL). To synthesize CaSiO$_3$ perovskite, we directly compressed the sample to 24 GPa. The sample was heated from both sides using a double-sided Nd:YLF laser heating system [*Prakapenka et al.*, 2008]. In each heating cycle, we collected the XRD patterns at temperatures ranging from 1200 K to approximately 2600 K at every 200 K steps at each given pressure from 24 GPa up to 156 GPa (Figures 1 and 2). By fitting the collected thermal radiation spectrum using the Planck radiation function under the Graybody approximation, we determined the

Figure 3. Full width at half maximum (FWHM) of the 200 peak at high temperatures at a given pressure.

temperature of the heated sample at each P-T step with an uncertainty in temperature of 50–100 K [*Prakapenka et al.*, 2008]. After each heating cycle, we also collected the diffraction pattern of $CaSiO_3$ at 300 K. Comparing the XRD patterns collected at high temperatures with those obtained at 300 K provides crucial information on the structure of $CaSiO_3$ in the Earth's lower mantle.

3. Results

The diffraction patterns of $CaSiO_3$ have been collected from 1200 K to 2600 K up to 156 GPa (Figures 1 and 2). Analysis of the collected diffraction patterns at high pressures and temperatures above 1200 K shows diffraction lines matching the $CaSiO_3$ perovskite in the cubic structure together with the pressure standard, Pt, and pressure medium, NaCl/KCl (Figure 1). We further compared the XRD patterns collected at high temperatures with the one quenched to 300 K at each given pressure. In particular, we analyzed the width of the 200 peak of $CaSiO_3$ perovskite using the full width at half maximum (FWHM) (Figure 3). The FWHM of the 200 peak at high temperatures is apparently smaller than that at 300 K which can be well interpreted as the occurrence of the 004 and 220 peaks in the tetragonal structure.

The thermal elastic parameters of $CaSiO_3$ perovskite were calculated by fitting the obtained P-V data using the Mie-Grüneisen EoS (Table 1 and Figure 4), which can provide more reliable constraints on the thermoelastic parameters and allow the extrapolation of the thermoelastic parameters beyond the range of the experimental measurements in a more secure way [*Jackson and Rigden*, 1996]. In addition, the use of Mie-Grüneisen EoS makes the conversion between the isothermal and adiabatic conditions internally consistent [*Jackson and Rigden*, 1996]. The P-V-T thermal EoS can be described as

$$P = P_0 + P_{th}, \tag{1}$$

where P_0 is the pressure at the reference temperature, T_0. The expression for P_0 is the same as that in the third-order Birch-Murnaghan EoS:

$$P_0 = \frac{3}{2} K_{0T} \left[\left(\frac{V}{V_0}\right)^{-7/3} - \left(\frac{V}{V_0}\right)^{-5/3} \right] \left\{ 1 + \frac{3}{4} \left(K'_{0T} - 4\right) \left[\left(\frac{V}{V_0}\right)^{-2/3} - 1 \right] \right\}, \tag{2}$$

where K_{0T} (V_{0T}) is the isothermal bulk modulus (unit cell volume) at the reference temperature. In equation (1), P_{th} is the thermal pressure and related to the difference in the internal thermal energy, E_{th}, between temperature T and T_0:

$$P_{th}(V,T) = \frac{\gamma}{V} \left[E_{th}(V,T) - E_{th}(V,T_0) \right], \tag{3}$$

where γ is the Grüneisen parameter. The internal thermal energy at a given temperature is associated with the Debye temperature, θ_D, and can be calculated as follows:

$$E_{th}(V,T) = 9nRT \left(\frac{\theta_D}{T}\right)^{-3} \int_0^{\theta_D/T} \frac{x^3}{e^x - 1} dx, \tag{4}$$

where R is the gas constant and n is the number of the atoms in the mineral formula. The Grüneisen parameter and the Debye temperature, θ_D, at a given P-T condition are described as

$$\gamma = \gamma_0 \left(\frac{V}{V_0}\right)^q \tag{5}$$

Table 1. Experimental P-V-T Data of CaSiO₃ Perovskite

P (GPa)	T (K)	V (Å³)	P (GPa)	T (K)	V (Å³)	P (GPa)	T (K)	V (Å³)
21.8 (3)	1200	43.07 (7)	43.3 (5)	1600	40.69 (6)	43.1 (5)	2000	41.05 (4)
32.0 (4)	1200	41.73 (2)	44.2 (5)	1600	40.61 (3)	44.5 (5)	2000	40.91 (4)
40.0 (5)	1200	40.83 (4)	51.0 (6)	1600	39.87 (5)	45.5 (5)	2000	40.87 (6)
42.6 (5)	1200	40.54 (2)	60.4 (7)	1600	39.06 (2)	47.4 (5)	2000	40.57 (3)
45.5 (6)	1200	40.23 (2)	67.9 (8)	1600	38.48 (2)	51.7 (5)	2000	40.37 (3)
46.6 (6)	1200	40.1 (4)	74.5 (9)	1600	38.01 (7)	52.7 (5)	2000	40.35 (5)
51.0 (7)	1200	39.66 (4)	77.8 (9)	1600	37.65 (2)	55.2 (6)	2000	39.89 (3)
58.6 (8)	1200	39.05 (4)	80.5 (10)	1600	37.44 (4)	59.0 (6)	2000	39.66 (2)
65.5 (9)	1200	38.29 (1)	83.8 (10)	1600	37.19 (4)	70.9 (7)	2000	38.45 (7)
75.7 (10)	1200	37.46 (3)	85.8 (10)	1600	37.08 (3)	71.6 (7)	2000	38.42 (2)
88.4 (12)	1200	36.73 (4)	92.2 (11)	1600	36.6 (3)	76.0 (8)	2000	38.11 (4)
91.3 (13)	1200	36.47 (3)	93.1 (12)	1600	36.6 (7)	77.5 (8)	2000	37.95 (6)
102.7 (15)	1200	35.82 (5)	105.0 (13)	1600	35.94 (2)	82.5 (9)	2000	37.5 (4)
107.9 (16)	1200	35.5 (4)	111.1 (15)	1600	35.58 (6)	86.2 (9)	2000	37.18 (7)
113.8 (17)	1200	35.17 (3)	116.6 (15)	1600	35.24 (1)	90.4 (10)	2000	37.01 (6)
118.0 (18)	1200	34.95 (3)	120.0 (16)	1600	34.98 (10)	95.1 (10)	2000	36.61 (5)
132.5 (20)	1200	34.05 (4)	135.3 (19)	1600	34.12 (11)	106.0 (12)	2000	36.09 (5)
140.7 (22)	1200	33.75 (7)	143.2 (20)	1600	33.82 (5)	113.2 (13)	2000	35.63 (3)
21.2 (2)	1400	43.2 (2)	146.9 (21)	1600	33.6 (3)	118.2 (14)	2000	35.34 (4)
23.8 (3)	1400	43.05 (7)	32.4 (4)	1800	42.36 (3)	122.2 (15)	2000	35.05 (4)
26.9 (3)	1400	42.62 (2)	32.9 (4)	1800	42.17 (6)	136.7 (17)	2000	34.17 (3)
32.4 (4)	1400	41.94 (6)	33.0 (4)	1800	42.24 (5)	143.9 (18)	2000	33.9 (5)
33.4 (4)	1400	41.75 (5)	37.3 (4)	1800	41.65 (8)	151.2 (20)	2000	33.62 (2)
38.7 (4)	1400	41.11 (5)	40.6 (4)	1800	41.27 (2)	118.2 (14)	2000	35.34 (6)
42.7 (5)	1400	40.61 (3)	44.4 (5)	1800	40.77 (7)	122.2 (15)	2000	35.05 (5)
45.2 (5)	1400	40.34 (4)	47.8 (5)	1800	40.42 (7)	136.7 (17)	2000	34.17 (2)
52.0 (6)	1400	39.62 (4)	49.2 (5)	1800	40.21 (3)	143.9 (18)	2000	33.9 (14)
60.0 (7)	1400	39.01 (3)	53.5 (6)	1800	39.85 (9)	151.2 (20)	2000	33.62 (10)
66.8 (8)	1400	38.47 (5)	56.5 (6)	1800	39.64 (3)	72.8 (7)	2200	38.5 (10)
76.8 (10)	1400	37.57 (2)	60.6 (6)	1800	39.3 (3)	77.4 (8)	2200	38.13 (5)
88.9 (12)	1400	36.82 (6)	64.4 (7)	1800	38.83 (2)	143.9 (18)	2000	33.9 (14)
92.2 (12)	1400	36.57 (5)	70.8 (8)	1800	38.45 (3)	151.2 (20)	2000	33.62 (10)
92.2 (12)	1400	36.57 (2)	70.9 (8)	1800	38.45 (5)	72.8 (7)	2200	38.5 (10)
104.1 (14)	1400	35.89 (14)	75.4 (8)	1800	38.03 (10)	77.4 (8)	2200	38.13 (5)
109.1 (15)	1400	35.55 (10)	76.8 (9)	1800	37.92 (5)	79.4 (8)	2200	37.99 (6)
115.0 (16)	1400	35.25 (10)	78.4 (9)	1800	37.66 (4)	92.8 (10)	2200	36.91 (8)
119.0 (17)	1400	34.96 (5)	80.5 (9)	1800	37.59 (2)	95.3 (10)	2200	36.68 (1)
134.1 (20)	1400	34.09 (8)	89.2 (10)	1800	37.02 (6)	106.5 (11)	2200	36.07 (11)
141.8 (21)	1400	33.79 (6)	94.0 (11)	1800	36.6 (10)	113.5 (13)	2200	35.71 (5)
25.7 (3)	1600	43.07 (2)	106.0 (13)	1800	36 (4)	118.5 (13)	2200	35.37 (4)
29.5 (3)	1600	42.45 (4)	112.1 (14)	1800	35.62 (12)	135.2 (16)	2200	34.34 (3)
35.3 (4)	1600	41.74 (4)	116.7 (15)	1800	35.33 (7)	137.2 (16)	2200	34.24 (3)
35.3 (4)	1600	41.72 (9)	121.7 (15)	1800	35.01 (2)	145.3 (18)	2200	33.87 (7)
39.1 (4)	1600	41.24 (3)	135.9 (18)	1800	34.15 (4)	151.8 (19)	2200	33.62 (7)
39.4 (4)	1600	41.19 (3)	144.1 (19)	1800	33.86 (6)	139.5 (16)	2400	34.25 (6)
40.6 (4)	1600	41.09 (1)	149.5 (20)	1800	33.6 (7)	146.2 (17)	2400	33.95 (5)
40.6 (4)	1600	41.06 (5)	35.5 (4)	2000	42.27 (7)	150.4 (18)	2400	33.75 (5)
42.0 (5)	1600	40.96 (2)	36.3 (4)	2000	42.13 (4)	151.6 (17)	2600	33.83 (8)

and

$$\theta_D = \theta_{D0}\exp\left(-\frac{\gamma - \gamma_0}{q}\right), \tag{6}$$

where q is a volume independent constant. θ_0 and γ_0 are the Debye temperature and Grüneisen parameter at ambient conditions, respectively.

We fitted the obtained P-V data using the Mie-Grüneisen EoS with a fixed K_{0T}' of 4 (Figure 4 and Table 2). We have found that thermoelastic parameters derived from equations (1) to (6) for the cubic CaSiO₃ perovskite
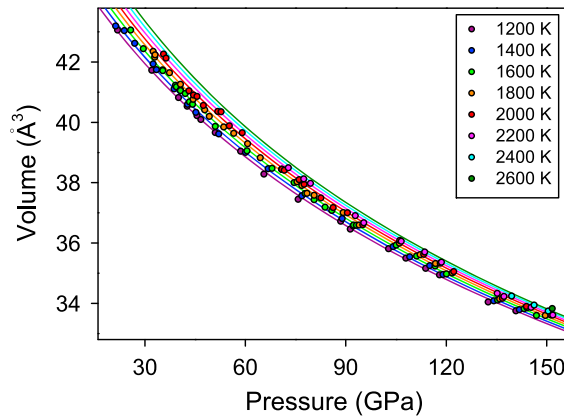
Figure 4. Pressure-volume relationship of cubic CaSiO$_3$ perovskite at high P-T. Circles: experimental data and lines: modeled results at various temperatures using the Mie-Grüneisen EoS (Table 2).

are not sensitive to the variation of θ_{D0}. Varying θ_{D0} from 1000 K to 1300 K only causes V_0 changing by 0.3 Å and does not affect the values of K_{0T}, γ_0, and q within experimental uncertainties (Table 2).

4. Discussion

The thermal EoS of cubic CaSiO$_3$ perovskite was investigated using both large-volume press and laser-heated DAC (LHDAC) with various pressure calibrants and scales in previous experimental studies [*Noguchi et al.*, 2013; *Ricolleau et al.*, 2009; *Shim et al.*, 2000; *Wang et al.*, 1996]. To directly compare the thermal EoS parameters of cubic CaSiO$_3$ perovskite in literature, we firstly recalculated pressures in these previous experimental data using the Pt scale of *Fei et al.* [2007a] and reanalyzed the P-V data in literature using the Mie-Grüneisen EoS with $K_{0T}' = 4$ (Table 3) [*Fei et al.*, 2007a; *Noguchi et al.*, 2013; *Shim et al.*, 2000]. The thermal EoS of cubic CaSiO$_3$ perovskite in previous study using large-volume press was investigated up to 13 GPa and 1600 K using the B1-NaCl phase as the pressure calibrant [*Wang et al.*, 1996]. We have also recalculated the pressures of the large-volume press study using the Mie-Grüneisen EoS of B1-NaCl in *Dorogokupets and Dewaele* [2007] which provides an internally consistent pressure scale of B1-NaCl with Pt [*Fei et al.*, 2007a]. As shown in Table 2, the thermoelastic parameters are not sensitive to the variation of θ_{D0}. We thus have used $\theta_{D0} = 1000$ K (fixed), which is an average value in literature [*Kawai and Tsuchiya*, 2014; *Zhang et al.*, 2006]. q was fixed to be 1 in two previous studies because of the limited experimental data points in *Shim et al.* [2000] and limited P-T range in *Wang et al.* [1996]. To compare with theoretical results, we recalculated the theoretical thermoelastic parameters using a reference temperature of 300 K, a fixed value of $\theta_{D0} = 1000$ and $K_{0T}' = 4$ (Table 2) [*Kawai and Tsuchiya*, 2014; *Zhang et al.*, 2006]. Since thermoelastic parameters of the cubic CaSiO$_3$ perovskite determined in a multicomponent system (KLB-1 peridotite) could be influenced by the element partitioning, we did not compare our derived thermoelastic parameters to the values reported in *Ricolleau et al.* [2009].

Using the obtained thermoelastic parameters, we have modeled ρ, K_T, and V_Φ of the cubic CaSiO$_3$ perovskite at lower mantle pressures along an expected mantle geotherm and compared them with recent literature results (Figure 5) [*Brown and Shankland*, 1981; *Kawai and Tsuchiya*, 2014; *Noguchi et al.*, 2013; *Shim et al.*, 2000; *Zhang et al.*, 2006]. Our obtained ρ of the cubic CaSiO$_3$ perovskite is most consistent with the theoretical prediction results by *Zhang et al.* [2006]. K_T of the cubic CaSiO$_3$ perovskite derived from our experimental results is almost the same as those of PREM within uncertainties, and the difference between our calculated V_Φ and that of PREM is less than 0.2(±0.4) km/s (Figure 5). The ρ profile calculated using the thermoelastic parameters of *Shim et al.* [2000] is lower than our results and other studies [*Kawai and Tsuchiya*, 2014; *Noguchi et al.*, 2013; *Zhang et al.*, 2006], largely due to their greater value of V_0 at ambient conditions. Meanwhile, a greater value of K_T and V_Φ of *Shim et al.* [2002] mainly results from an anomalous small γ_0 value (Table 3). The thermal EoS parameters of *Shim et al.* [2002] were obtained from the P-V-T data up to 69 GPa and 2380 K. Relatively limited P-T range could be the potential cause for the difference in the thermal EoS parameters as compared to this study. Although the calculated ρ in *Wang et al.* [1996] is consistent with our results, their K_T and V_Φ profiles are 4–8(±0.9)% lower. We should mention that the P-V-T data of

Table 2. Thermoelastic Parameters of Cubic CaSiO$_3$ Perovskite

	Model 1	Model 2	Model 3
K_{0T} (GPa)	249 (4)	249 (4)	249 (4)
K_{0T}'	4 (fixed)	4 (fixed)	4 (fixed)
V_0 (Å^3)	45.4 (1)	45.1 (1)	45.6 (1)
θ_0 (K)	1000 (fixed)	1300 (fixed)	1500 (fixed)
γ_0	1.8 (2)	1.8 (2)	1.9 (2)
q	1.1 (4)	1.0 (4)	1.0 (4)

Table 3. Thermoelastic Parameters of Cubic $CaSiO_3$ Perovskite

	This Study	Wang 1996	Noguchi 2013	Shim 2000	Zhang 2006	Kawai 2013
K_{0T} (GPa)	249 (4)	237(9)	208(8)	248 (13)	250 (1)	227 (1)
K_{0T}'	4 (fixed)	4 (fixed)	4 (fixed)	4 (fixed)	4 (fixed)	4 (fixed)
V_0 (Å³)	45.4 (1)	45.6(1)	46.1(3)	46.6 (3)	45.65 (2)	45.51 (2)
θ_0 (K)	1000	1000	1000	1000	1000	1000
γ_0	1.8 (2)	1.8(3)	2.3 (3)	0.96 (23)	1.64 (3)	1.58 (2)
q	1.1 (4)	1(fixed)	0.97(27)	1(fixed)	1.43 (7)	1.31 (5)
Technique[a]	LHDAC	DIA-6	LHDAC + EHDAC	LHDAC	Theory	Theory
P_{max} (GPa)	151	13	127	96		
T_{max} (K)	2600	1600	2300	2419		
P. Medium	KCl + NaCl	NaCl	NaCl	NaCl + Ar		
P. Calibrant	Pt	NaCl	Pt	Pt		

[a]LHDAC: laser-heated DAC and EHDAC: externally heated DAC.

$CaSiO_3$ perovskite in *Wang et al.* [1996] was obtained using the energy-dispersive XRD technique which typically gives a lower resolution in the diffraction peaks than the angle-dispersive XRD technique used here. Nearly half of the P-V-T data in *Wang et al.* [1996] were collected below 10 GPa and 600 K which is outside the stability field of the cubic $CaSiO_3$ perovskite [*Stixrude et al.*, 2007]. Considering the small difference in the diffraction patterns between tetragonal and cubic $CaSiO_3$ perovskite (Figure 2), it could be quite difficult to identify the potential back transformation of the cubic $CaSiO_3$ perovskite to the lower P-T phase using the energy-dispersive XRD technique, leading to greater uncertainties in the derived thermal EoS parameters [*Wang et al.*, 1996]. In addition, due to a significantly low K_{0T} value, K_T and V_Φ calculated using the thermoelastic parameters of *Noguchi et al.* [2013] are significantly lower than our results and other literature values, whereas ρ exhibits a much greater slope with pressure. The difference in K_T and V_Φ between our modeled results and that of *Noguchi et al.* [2013] is as large as 22% and 18%, respectively, at lower mantle P-T conditions. Thermoelastic parameters of $CaSiO_3$ perovskite in *Noguchi et al.* [2013] were derived by fitting the experimental P-V data along three different isotherms. Although data at 700 K were obtained using the externally heated DACs, other data at 1600 K and 2100 K were obtained using laser-heated DACs which could suffer from similar experimental uncertainties as this study [*Noguchi et al.*, 2013]. However, limited measurements at high P-T and deviation between the experimental data and the fitting line at 1600 K could lead to great uncertainties in the thermal elastic parameters, ρ, K_T, and V_Φ of $CaSiO_3$ perovskite [*Noguchi et al.*,

Figure 5. Modeled density (ρ), isothermal bulk modulus (K_T), and bulk sound velocity (V_Φ) of $CaSiO_3$ perovskite along a representative mantle geotherm. Red line: this study; blue dashed line: *Noguchi et al.* [2013]; blue dashed-dotted line: *Shim et al.* [2000]; blue dotted line: *Kawai and Tsuchiya* [2014]; and black line: PREM [*Dziewonski and Anderson*, 1981].

2013]. In a theoretical study, *Kawai and Tsuchiya* [2014] predicted a much greater ρ and lower K_T and V_Φ profile of $CaSiO_3$ perovskite than our results and another theoretical study of *Zhang et al.* [2006]. Although both *Zhang et al.* [2006] and *Kawai and Tsuchiya* [2014] used molecular dynamic simulations to study the thermoelastic EoS of $CaSiO_3$ perovskite, thermoelastic parameters as well as the ρ, K_T, and V_Φ profiles of $CaSiO_3$ perovskite in *Zhang et al.* [2006] are more consistent with our experimental results.

5. The EoS of Bridgmanite and Ferropericlase

5.1. Bridgmanite

Based on previous studies, the lower mantle bridgmanite is assumed to have an average composition of $Mg_{0.9}Fe_{0.1}Al_{0.1}Si_{0.9}O_3$ (Al-Bm10) in our modeling [*Irifune et al.*, 2010; *Ringwood*, 1975]. Since the presence of Al will greatly limit the amount of B site Fe^{3+}, which will undergo the HS to LS transition, and the experimental constraints on the EoS parameters of bridgmanite with the LS Fe^{3+} are significantly limited, we thus did not consider the effect of Fe spin transition on the EoS parameters of bridgmanite [*Catalli et al.*, 2011; *Dobson and Brodholt*, 2005; *Mao et al.*, 2015].

We have reevaluated the literature data for the EoS parameters of bridgmanite in the Fe-diluted system because the lower mantle bridgmanite is expected to contain ~10% Fe and 10% Al (Table 4). The EoS of bridgmanite is mainly studied by DAC together with synchrotron XRD techniques using either Au, Pt, or Ruby pressure scales (Table 4). Experiments using polycrylline bridgmanite samples in various pressure medium have performed laser-annealing at high pressures to reduce the deviatoric stress, whereas single-crystal studies used a softer pressure medium, He, and conducted measurements at 300 K (Table 4). To directly comparing the results in previous high-P studies, we have reanalyzed the pressures in literature using the self-consistent pressure scale of *Fei et al.* [2007a]. Pressures in previous studies using Au as the pressure calibrant and the pressure scale of *Tsuchiya* [2003] were recalculated using the Au scale of *Fei et al.* [2007a] [*Catalli et al.*, 2011; *Lundin et al.*, 2008; *Nishio-Hamane et al.*, 2008]. Ruby has also been used as the pressure calibrant [*Andrault et al.*, 2001; *Ballaran et al.*, 2012]. We have also recalculated the pressure using the Ruby pressure scale of *Dewaele et al.* [2004] which is most consistent with the metal pressure scales in *Fei et al.* [2007a] (Table 4) [*Andrault et al.*, 2001; *Ballaran et al.*, 2012]. We should note that the obtained K_{T0} after the recalibration spreads in values across studies, indicating a greater uncertainty of K_{T0} in existing high-pressure experiments.

K_{0T} suffers from a well-known tradeoff with K_{0T}'. To have a direct comparison between different studies for various compositions, we analyzed the P-V data of bridgmanite in literature to obtain K_{0T} with a fixed $K_{0T}' = 4$. It is shown that ρ_0 of Fe-bearing bridgmanite increases linearly with increasing Fe content, while K_{0T} does not show a notable change with increasing Fe content within experimental uncertainties (Figure 6). However, the combined effect of Fe and Al in the Fe-diluted system is less well constrained due to limited experimental studies and conflicting results in the literature [*Andrault et al.*, 2001; *Catalli et al.*, 2011; *Nishio-Hamane et al.*, 2008; *Saikia et al.*, 2009; Mao et al., submitted manuscript, 2016]. Here the net effect of Fe and Al on ρ_0 and K_{0T} of bridgmanite is mainly considered using the high-quality single-crystal XRD results of Mao et al. (submitted manuscript, 2016). We simply assumed that ρ_0 of bridgmanite is mainly controlled by the amount of Fe, while K_{0T} is independent of the Fe content and follows a linear increase with the Al content (Table 4) (Mao et al., submitted manuscript, 2016):

$$\rho_{0\_Pv} = 4.11 + 1.07X_{Fe} + 0.11X_{Al}$$

$$K_{0T\_Pv} = 253 + 100X_{Al}, \tag{7}$$

where $X_{Fe} = Fe/(Fe + Mg)$ and $X_{Al} = Al/(Al + Si)$.

A survey of the literature indicates that experimental studies on the thermoelastic parameters of bridgmanite remain to be reconciled including the Fe and Al compositional effects on the EoS parameters [*Fiquet et al.*, 2000; *Tange et al.*, 2012; *Wolf et al.*, 2015]. Here we have examined how the variations in the values of θ_{D0}, γ_0, and q reported in literature could influence the modeled ρ and V_Φ profiles of bridgmanite. We modeled ρ and V_Φ of Al-Pv10 along a typical lower mantle geotherm using equations (1)–(6) together with literature thermoelastic parameters [*Fiquet et al.*, 2000; *Tange et al.*, 2012; *Wolf et al.*, 2015]. Our modeling results show that using different literature thermoelastic parameters can result in about 0.4(±0.5)% difference in the ρ and V_Φ profiles [*Fiquet et al.*, 2000; *Tange et al.*, 2012; *Wolf et al.*, 2015]. Considering the content of bridgmanite in the

Table 4. Experimental Thermal Equation of State (EoS) Parameters of Major Lower Mantle Minerals

Minerals	Composition	Technique	Sample	P. Calibrant	P. Medium	T (K)	P$_{max}$ (GPa)
HS. Fp	$(Mg_{0.8}Fe_{0.2})O$	DAC	powder	NaCl	NaCl	300	40
	$(Mg_{0.75}Fe_{0.25})O$	LHDAC	powder	Au	NaCl + KCl	300	140
	$(Mg_{0.65}Fe_{0.35})O$	DAC	powder	Ruby	Ne	300	126
	$(Mg_{0.94}Fe_{0.06})O$		single-crystal			300	1 bar
	$(Mg_{0.85}Fe_{0.15})O$		single-crystal			300	1 bar
	$(Mg_{0.76}Fe_{0.24})O$		single-crystal			300	1 bar
	$(Mg_{0.73}Fe_{0.27})O$		single-crystal			300	1 bar
LS. Fp	MgO		powder			300	1 bar
	$(Mg_{0.8}Fe_{0.2})O$	DAC	powder	NaCl	NaCl	300	40
	$(Mg_{0.75}Fe_{0.25})O$	LHDAC	powder	Au	NaCl + KCl	300	140
	$(Mg_{0.65}Fe_{0.35})O$	DAC	powder	Ruby	Ne	300	126
Bm	$MgSiO_3$	DAC	single-crystal	Ruby	He	300	75
	$(Mg_{0.96}Fe_{0.04})SiO_3$	DAC	single-crystal	Ruby	He	300	75
	$(Mg_{0.94}Fe_{0.06})SiO_3$	DAC	single-crystal	Pt	He	300	85
	$(Mg_{0.9}Fe_{0.1})SiO_3$		powder	Pt		300	1 bar
	$(Mg_{0.91}Fe_{0.09})SiO_3$	LHDAC	powder	Au	Ar	300	86
	$(Mg_{0.85}Fe_{0.15})SiO_3$	LHDAC	powder	Au	Ar	300	110
	$(Mg_{0.95}Fe_{0.05})SiO_3$	LHDAC	powder	Ruby	Ar	300	70
	$(Mg_{0.91}Fe_{0.09})SiO_3$	LHDAC	powder	Pt	Ne + NaCl	300	77
	$Mg_{0.6}Fe_{0.41}Al_{0.36}Si_{0.62}O_3$	DAC	single-crystal	Ruby	He	300	75
	$Mg_{0.6}Fe_{0.4}Al_{0.37}Si_{0.63}O_3$	LHDAC	single-crystal	Ne	Ne	300	80
	$Mg_{0.95}Fe_{0.05}Al_{0.05}Si_{0.95}O_3$	LHDAC	powder	Ruby	Ar	300	70
	$Mg_{0.89}Fe_{0.12}Al_{0.11}Si_{0.89}O_3$	DAC	single-crystal	Pt	He	300	130
	$Mg_{0.85}Fe_{0.15}Al_{0.15}Si_{0.85}O_3$	LHDAC	powder	Au	NaCl	300	143
	$Mg_{0.88}Fe_{0.13}Al_{0.11}Si_{0.88}O_3$	LHDAC	powder	Au	Ar	300	95

pyrolitic lower mantle to be 75%, the ρ and V_Φ profiles of Al-Pv10 calculated using different thermoelastic parameters will differ by ~0.3(±0.5)%. Here the thermal EoS parameters of Al-Pv10 bridgmanite used in our following modeling are listed in Table 5.

5.2. Ferropericlase

In our modeling, ferropericlase in the lower mantle is assumed to have a composition of $(Mg_{0.83}Fe_{0.17})O$ (Fp17) [*Irifune et al.*, 2010; *Ringwood*, 1975]. It is well known that Fe in ferropericlase will transform from the HS to LS state at lower mantle P-T conditions which can influence the EoS parameters of ferropericlase in the region [e.g., *Badro et al.*, 2003; *Crowhurst et al.*, 2008; *Lin et al.*, 2013; *Marquardt et al.*, 2009b; *Wentzcovitch et al.*, 2009]. To directly compare results from different studies using various pressure scales and derive the effect of Fe on the thermoelastic parameters of ferropericlase, we also recalculated the pressure of literature data using the self-consistent pressure scale (Table 4) [*Fei et al.*, 2007a]. Similar to the analysis of bridgmanite, pressures in the literature using either Pt or Au were recalculated using the internally consistent pressure scale of [*Fei et al.*, 2007a], whereas pressures determined by the fluorescence of Ruby were recomputed using the pressure scale of *Dewaele et al.* [2004]. We limit the Fe content in ferropericlase of literature data up to 40% because ferropericlase in the lower mantle is assumed to have a composition of Fp17 [*Irifune et al.*, 2010; *Ringwood*, 1975]. We fitted the relevant literature P-V data at 300 K using the third-order Birch-Murnaghan EoS to constrain K_{0T} of ferropericlase with fixed $K_{0T}' = 4$ in both HS and LS states (Figure 6). V_0 was also fixed using the experimental values obtained at ambient conditions. The effect of Fe on ρ_0 and K_{0T} of the LS ferropericlase is evaluated using three experimental results [*Chen et al.*, 2012; *Fei et al.*, 2007b; *Mao et al.*, 2011a] because the P-V data in other experimental studies are quite limited and cannot be used to provide reliable constraints on the EoS parameters of LS ferropericlase [*Komabayashi et al.*, 2010; *Lin et al.*, 2005; *Marquardt et al.*, 2009a; *Speziale et al.*, 2007].

We have noted that ρ_0 of both HS and LS ferropericlase increases linearly with the Fe content (Figure 6). K_{0T} of the HS ferropericlase was found to be independent of the Fe content when the molar percentage of Fe in ferropericlase is less than 25% (Figure 6) [*Jacobsen et al.*, 2002]:

$$\rho_{0\_HS-Fp} = 3.57 + 2.48 X_{Fe},$$

$$K_{0T\_HS-Fp} = 159, \tag{8}$$

Table 4. (continued)

Original Data				Recalibrated Data			
V_0 (Å^3)	K_0 (GPa)	K'	ρ_0 (g/cm^3)	K_0 (GPa)	K'	ρ_0 (g/cm^3)	References
74.2(1)	170(3)	4	4.17(1)	170(3)	4	4.17(1)	*Fei et al.* [2007b]
74.4(6)	166(7)	4	4.3(3)	166(7)	4	4.3(3)	*Mao et al.* [2011b]
72.9 (1.3)	182(17)	4	4.68(8)	181(12)	4	4.63(9)	*Chen et al.* [2012]
75.10(1)			3.723(8)			3.723(8)	*Jacobsen et al.* [2002]
75.63(1)			3.948(6)			3.948(6)	*Jacobsen et al.* [2002]
76.34(1)			4.157(6)			4.157(6)	*Jacobsen et al.* [2002]
76.34(1)			4.227(14)			4.227(14)	*Jacobsen et al.* [2002]
74.7(3)	160(3)	4	3.57(1)				*Jacobsen et al.* [2002]
74.2(1)	170(3)	4	4.17(1)	170(3)	4	4.17(1)	*Fei et al.* [2007b]
74.4(6)	166(7)	4	4.3(3)	166(7)	4	4.3(3)	*Mao et al.* [2011b]
72.9 (1.3)	182(17)	4	4.68(8)	181(12)	4	4.63(9)	*Chen et al.* [2012]
162.36 (4)	251(2)	4.11(7)	4.108(1)	251(2)	4	4.110(2)	*Ballaran et al.* [2012]
163.09(6)	253(2)	3.99(7)	4.141(1)	250(2)	4	4.141(2)	*Ballaran et al.* [2012]
162.96(1)	255(2)	4	4.170(1)	255(2)	4	4.170(1)	Mao et al. (submitted manuscript, 2016)
162.6(3)			4.231(7)	--			*Mao et al.* [2015]
163.18(3)	257(1)	4	4.203(1)	251(1)	4	4.203(1)	*Lundin et al.* [2008]
163.3(7)	257(1)	4	4.277(2)	254(1)	4	4.277(2)	*Lundin et al.* [2008]
162.7(1)	255.4	4	4.164(1)	260(2)	4	4.164(1)	*Andrault et al.* [2001]
163	251(13)	4	4.21	251(13)	4	4.21	*Dorfman et al.* [2013]
168.93(5)	240(2)	4.12(8)	4.429(1)	240(1)	4	4.43(4)	*Ballaran et al.* [2012]
169.9(3)	233(4)	4	4.403(8)	233(3)	4	4.403(8)	*Glazyrin et al.* [2014]
163.2(3)	265(4)	4	4.149(1)	265(4)	4	4.149(1)	*Andrault et al.* [2001]
164.05(1)	264	4	4.224(4)	264(1)	4	4.224(4)	Mao et al. (submitted manuscript, 2016)
164.96(18)	252(1)	4	4.227(5)	242(4)	4	4.230(1)	*Nishio-Hamane et al.* [2008]
162(1)	269(13)	4	4.28(3)	232(4)	4	4.21(2)	*Catalli et al.* [2011]
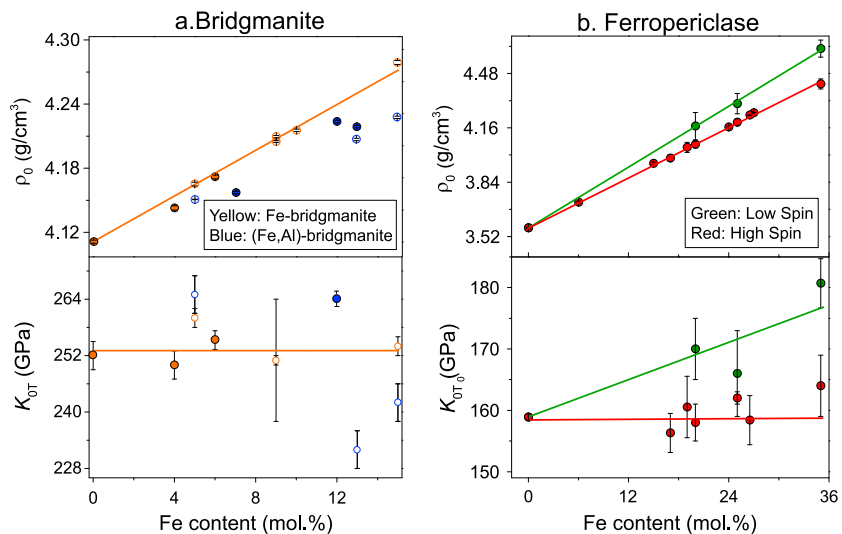
Figure 6. Density (ρ_0) and isothermal bulk modulus (K_{0T}) of bridgmanite and ferropericlase at ambient conditions. (a) Bridgmanite and (b) ferropericlase. Open orange circles and line: polycrystalline Fe-bridgmanite [*Andrault et al.*, 2001; *Catalli et al.*, 2010; *Dobson and Brodholt*, 2005; *Dorfman et al.*, 2013; *Lundin et al.*, 2008]; solid orange circles: single-crystal Fe-bridgmanite [*Ballaran et al.*, 2012; Mao et al., submitted manuscript, 2016]; open blue circles: polycrystalline (Fe, Al)-bridgmanite [*Andrault et al.*, 2001; *Catalli et al.*, 2011; *Nishio-Hamane et al.*, 2008]; solid blue circles: single-crystal (Fe, Al)-bridgmanite [*Saikia et al.*, 2009; Mao et al., submitted manuscript, 2016]; red circles and line: HS ferropericlase [*Fei et al.*, 2007b; *Jacobsen et al.*, 2002; *Komabayashi et al.*, 2010; *Lin et al.*, 2005; *Mao et al.*, 2011a; *Marquardt et al.*, 2009a; *Speziale et al.*, 2007]; and green circles and line: LS ferropericlase [*Fei et al.*, 2007b; *Mao et al.*, 2011a].

where $X_{Fe} = Fe/(Fe + Mg)$. The HS to LS transition of Fe^{2+} in ferropericlase will cause a sudden drop in the unit cell volume because of a smaller ionic radius of the LS Fe^{2+}. Both theoretical and experimental studies have found that K_{0T} of the LS ferropericlase is greater than that of the HS phase with the same amount of Fe content, indicating that the LS Fe^{2+} with a smaller ionic radius is more incompressible than the HS Fe^{2+}. K_{0T} of ferropericlase exhibits a positive dependence on the amount of LS Fe^{2+}. Since reliable experimental constraints on K_{0T} of the LS ferropericlase are limited [*Chen et al.*, 2012; *Fei et al.*, 2007b; *Mao et al.*, 2011a], we assumed a linear relationship between K_{0T} and the LS Fe content in ferropericlase:

$$\rho_{0\_LS-Fp} = 3.57 + 2.95X_{Fe}$$

$$K_{0T\_LS-Fp} = 159 + 0.36X_{Fe}. \tag{9}$$

We note that the thermal EoS of ferropericlase is not available for Fp17 but is well constrained for Fp25 [*Mao et al.*, 2011a]. Here we refitted the high P-T-V data of Fp25 using the Mie-Grüneisen EoS to obtain the thermal EoS parameters of both HS and LS Fp25, which are then compositional-corrected for obtaining the thermal EoS parameters of Fp17 in our modeling. It should be noted that θ_{D0} of Fp25 cannot be well constrained from the experimental P-V relationships [*Mao et al.*, 2011a]. We thus fixed $\theta_{D0} = 763$ K which is the value used for Mie-Grüneisen EoS modeling of the experimental P-V-T data of MgO [*Speziale et al.*, 2001]. θ_{D0}, γ_0, and q of Fp17 were assumed to be the same as those of Fp25 (Table 5). The width and the onset of the Fe spin transition in ferropericlase do not show an obvious dependence on the Fe content [*Lin et al.*, 2013]. The P-T conditions of the spin crossover for Fp17 along a mantle geotherm thus have been assumed to the same as Fp25 [*Mao et al.*, 2011a].

6. Modeling ρ, K_S, and V_Φ of the Lower Mantle

In this section, we used the thermal EoS parameters of bridgmanite, ferropericlase, and $CaSiO_3$ perovskite to model the ρ, K_S, and V_Φ profiles of a lower mantle with a pyrolitic composition or a chondritic composition (Tables 3 and 5 and Figure 7). Here we limited all of our models up to 120 GPa (2600 km depth) which is several hundred kilometers above the core-mantle boundary, because the thermal structure and mineralogy in the region, especially in the D″ zone, are quite different from the expected lower mantle geotherm.

6.1. Seismic Profile of a Pyrolitic Lower Mantle

We firstly considered a lower mantle with a pyrolitic composition and modeled ρ, K_S, and V_Φ of the lower mantle with a volume ratio of 75% bridgmanite, 17% ferropericlase, and 8% $CaSiO_3$ perovskite using Voigt-Reuss-Hill average along an expected mantle geotherm (Figure 7) [*Brown and Shankland*, 1981; *Cottaar et al.*, 2014; *Ringwood*, 1975]. Excluding the bottom several hundred kilometers above the core-mantle boundary, both V_P and V_S of the lower mantle increase almost in a constant gradient, indicating weak lateral variations and relative simple structure of the lower mantle [e.g., *Dziewonski and Anderson*, 1981; *Garnero and McNamara*, 2008; *Lay et al.*, 1998]. Standard seismic 1-D model, such as PREM, is thus a good representative seismic average of the lower mantle, except in the lowermost few hundred kilometers and some seismically heterogeneous regions. Therefore, we have used it for comparison with our modeling results. It shows that ρ of a pyrolitic lower mantle is in an excellent agreement with ρ of PREM; the difference in ρ between them is within 0.2(±0.2)%. Our modeled ρ of a pyrolitic lower mantle is also consistent with the experimentally obtained density of pyrolite and the theoretical predicted results [*Wang et al.*, 2015]. The density of a natural KLB-1 peridotite, which has a composition close to the pyrolite model, was investigated up to 120 GPa and 2000 K [*Ricolleau et al.*, 2009]. However, ρ at less than 90 GPa in *Ricolleau et al.* [2009] is lower than our modeled results and theoretical calculations, which is caused by the relatively low density of ferropericlase [*Wang et al.*, 2015; *Zhang et al.*, 2016]. The thermal EoS parameters in *Ricolleau et al.* [2009] for each lower mantle minerals were constrained from limited high P-T XRD measurements, which can result great uncertainties in the modeled ρ of the lower mantle in a pyrolitic composition.

Similar to the behavior of ρ, both K_S and V_Φ profiles of a pyrolitic composition in our modeling are in general agreement with those of PREM (Figure 7). Except the spin crossover in ferropericlase, the difference in K_S between the pyrolitic mantle and PREM is within ±0.8(±1.2)%. The spin transition of Fe in ferropericlase causes a great softening in K_S between 75 and 120 GPa and increase the difference in K_S between our pyrolitic model and PREM up to 3(±1.2)%. The difference in V_Φ between our pyrolitic model and PREM is within 1.6 (±0.9)% in the lower mantle. Similar softening in K_S and V_Φ in a pyrolitic lower mantle due to the spin transition

Table 5. Thermoelastic Parameters of Bridgmanite and Ferropericlase

	Bridgmanite[a] $Mg_{0.9}Fe_{0.1}Al_{0.1}Si_{0.9}O_3$	Fp $(Mg_{0.83}Fe_{0.17}O)$[b]	
		HS	LS
K_{0T} (GPa)	262 (3)	159 (1)	165(4)
K_{0T}'	4 (fixed)	4 (fixed)	4 (fixed)
V_0 (Å^3)	163.8 (5)	76.1 (3)	74.4 (5)
θ_0 (K)	1100 (fixed)	763 (fixed)	763 (fixed)
γ_0	1.4 (1)	1.4(1)	1.5(4)
q	1.1 (1)	0.16 (14)	0.01(1)

[a]*Fiquet et al.* [2000] and *Mao et al.* [2015].
[b]*Mao et al.* [2011a].

of Fe in ferropericlase has also been proposed in previous theoretical calculation [*Wentzcovitch et al.*, 2009]. The anomalous variation in K_S and V_Φ of our modeled pyrolitic lower mantle extending down to ~800 km depth is not shown in PREM potentially due to the limited spatial resolution in PREM over a wide pressure (depth) range.

Here we have also tested how the variation in the composition of bridgmanite and ferropericlase as well as temperature affects the ρ, K_S, and V_Φ profiles using the aforementioned pyrolite model as the reference (Figure 8) [*Irifune et al.*, 2010]. These analyses could help decipher possible lateral chemical and thermal heterogeneities in the lower mantle as indicated by recent seismic studies [e.g., *Ishii and Tromp*, 2004; *Ni et al.*, 2002; *Trampert et al.*, 2004; *Wang and Wen*, 2007]. The modeling was performed at three pressures: 40 GPa before the spin transition of ferropericlase; 90 GPa in the spin crossover; and 120 GPa after the completion of the spin transition (Figure 8). The Fe content in bridgmanite is allowed to vary from 7 mol % (Al-Bm7) to 15 mol % (Al-Bm15). With a fixed Fe partition coefficient between bridgmanite and ferropericlase of 0.54, we calculated the Fe content in ferropericlase accordingly. The Al content in bridgmanite is fixed to be 10 mol %. Meanwhile, we have tested a ±500 K variation in temperature using an expected mantle geotherm as the reference (Figure 7) [*Brown and Shankland*, 1981]. At all the investigated pressures, our modeling results show that varying the Fe content in bridgmanite by ±1 mol % will result in a ±0.5(±0.2)% variation in ρ, but only a ±0.2% variation in V_Φ with a fixed temperature. With a fixed Fe content, varying the temperature by ±100 K will lead to a ±0.2 (±0.2)% variation in both ρ and V_Φ. In this case, the lateral variation in the chemical composition has a stronger effect on ρ but only weakly affects the V_Φ profile of the lower mantle. The variation in temperature has similar effect on ρ and V_Φ. Considering the uncertainties of these parameters in our mineral physics modeling as well as seismic profiles, the temperature variations and a small change in Fe content in bridgmanite, such as shown in *Irifune et al.* [2010], are likely to be undetectable in one-dimensional seismic studies.

6.2. Seismic Profile of a Chondritic Lower Mantle

Assuming a Si-enriched lower mantle, we have constructed the ρ, K_S, and V_Φ profiles of a lower mantle with two chondritic compositions along an expected mantle geotherm using Voigt-Reuss-Hill average (Figure 8) [*Brown and Shankland*, 1981; *Watt et al.*, 1976]: (1) Model M1, consisted of 85 vol % bridgmanite, 7 vol % ferropericlase, and 8 vol % CaSiO$_3$ perovskite with an Mg/Si ratio of 1 [*Anderson*, 1989] and (2) Model M2, assuming that the lower mantle is depleted in ferropericlase, which is used to test the seismic signature of a Si highly enriched lower mantle with an Mg/Si ratio of 0.91. Model M2 is composed solely of 92% bridgmanite and 8% CaSiO$_3$ perovskite.

We note that lower mantle with a chondritic composition has a ρ profile less consistent with PREM than lower mantle with a pyrolitic composition (Figure 8). Elevating the Si content in the lower mantle from a pyrolitic composition to our model M1 with an Mg/Si ratio of 1 results in ρ ~0.4(±0.2)% greater than PREM at 24 GPa. Although the difference in ρ between our model M1 and PREM decreases with pressure and reaches a minimum of 0 at 57 GPa, it starts to increase with pressure above 57 GPa and reaches ~0.4(±0.2)% at 120 GPa (Figure 8). The lower mantle, if depleted in ferropericlase, as shown in our model M2, will have a ρ ~0.8(±0.2)% greater than PREM at 120 GPa (Figure 8). As a result, the ρ profile of the lower mantle with a chondritic composition will be less consistent with PREM as compared to a pyrolitic lower mantle. Moreover, elevating the Si content also deviates K_S and V_Φ of the lower mantle away from those of PREM. K_S and V_Φ in both model M1 and M2 in a chondritic composition exhibit stronger deviations from PREM than a pyrolitic lower mantle [*Dziewonski and Anderson*, 1981].
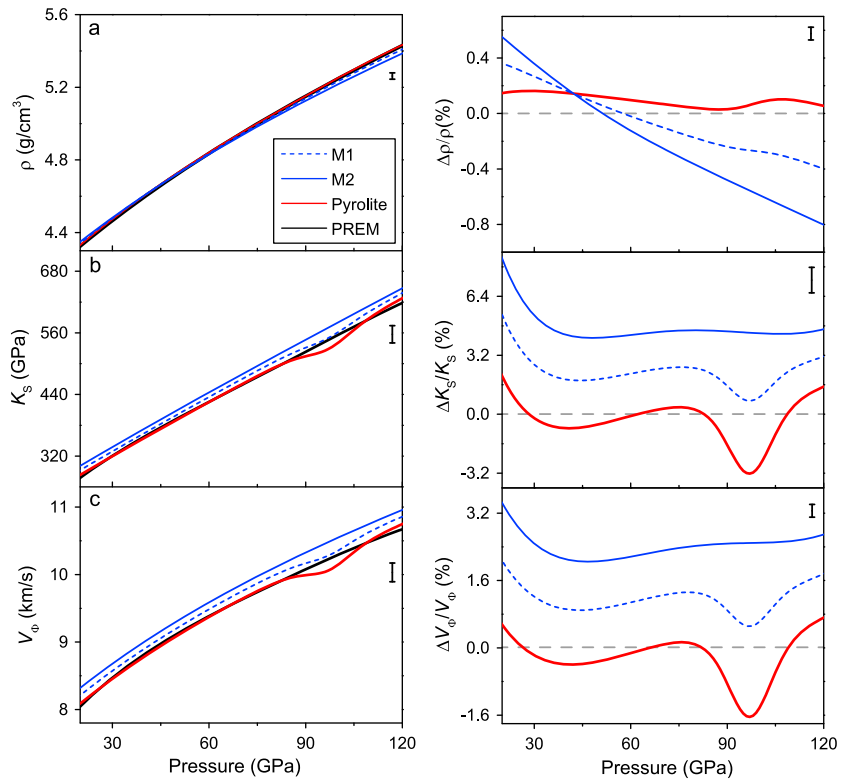
Figure 7. Modeled density (ρ), isothermal bulk modulus (K_T), and bulk sound velocity (V_Φ) of the lower mantle. Black line: PREM [*Dziewonski and Anderson*, 1981]; red line: predictions for a pyrolitic lower mantle; blue dashed lines: chondritic model M1 with an Mg/Si ratio of 1 which is consisted of 85% bridgmanite, 7% ferropericlase, and 8% $CaSiO_3$ perovskite; and blue solid line: chondritic model M2, depleted in ferropericlase with 92% bridgmanite and 8% $CaSiO_3$ perovskite.

6.3. Influence of $CaSiO_3$ Perovskite on Seismic Profiles

Owing to lack of experimental constraints on the high P-T sound velocity of $CaSiO_3$ perovskite, some previous studies have neglected the contribution of $CaSiO_3$ perovskite to the ρ and velocity profiles of the lower mantle [*Murakami et al.*, 2007, 2012; *Wang et al.*, 2015]. Here we have examined how the variation in the fraction of $CaSiO_3$ perovskite affects the ρ, K_S, and V_Φ profiles of the lower mantle in order to understand potential seismic signatures of $CaSiO_3$ perovskite in the region.

Assuming that the relative volume ratio between ferropericlase and bridgmanite is the same as that of a pyrolitic mantle, we have constructed two ρ, K_T, and V_Φ models of the lower mantle with different $CaSiO_3$ perovskite contents (Figure 9): (1) Model M3 with 0% $CaSiO_3$ perovskite and (2) Model M4, 16% $CaSiO_3$ perovskite content in the pyrolitic mantle that is approximately doubled from a typical content. Our modeled results show that decreasing the amount of $CaSiO_3$ perovskite will lower ρ, K_S, and V_Φ of the lower mantle. Although M3 with 0% $CaSiO_3$ perovskite has a density profile more consistent with PREM, the difference in density between M3 and the pyrolitic mantle is quite small. In addition, variation of the $CaSiO_3$ perovskite content has a negligible effect on the K_S and V_Φ of the lower mantle considering the uncertainties in our modeling. The variation in the fraction of $CaSiO_3$ perovskite thus may not be seismically detectable using the ρ and V_Φ profiles. These modeled results show that ρ and V_Φ profiles of the lower mantle mainly reflect the relative bridgmanite to ferropericlase ratio.

6.4. $R_{\rho/\Phi}$

The relative variation in the density and sound velocity, $R_{\rho/\Phi} = d \ln \rho / d \ln V_\Phi$, has been applied to understand the physical cause for the potential seismic and compositional heterogeneities in the Earth's mantle [e.g., *Romanowicz*, 2001; *Simmons et al.*, 2009]. Here we have modeled $R_{\rho/\Phi}$ of the candidate lower mantle minerals
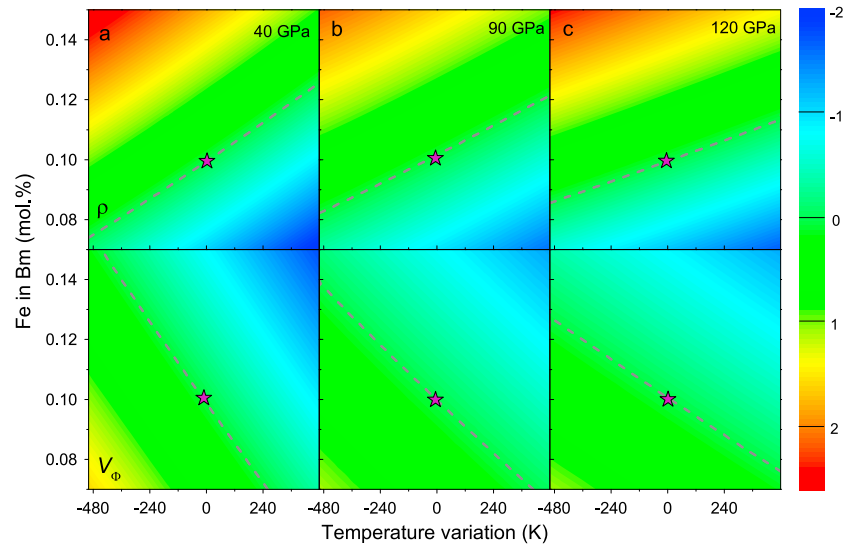
Figure 8. Density (ρ) and bulk sound velocity (V_Φ) variation of the lower mantle using those of a pyrolitic lower mantle as the reference. (a) 40 GPa, (b) 90 GPa, and (c) 120 GPa. Bm: bridgmanite. The star indicates ρ and V_Φ of a pyrolitic lower mantle along a normal mantle geotherm [*Brown and Shankland*, 1981]. The variation in temperature is considered using the normal mantle geotherm as the reference [*Brown and Shankland*, 1981]. The dashed line represents the zero value. Our modeling also shows the tradeoff between temperature and Fe content in lower mantle minerals on the ρ and V_Φ profiles of the lower mantle.
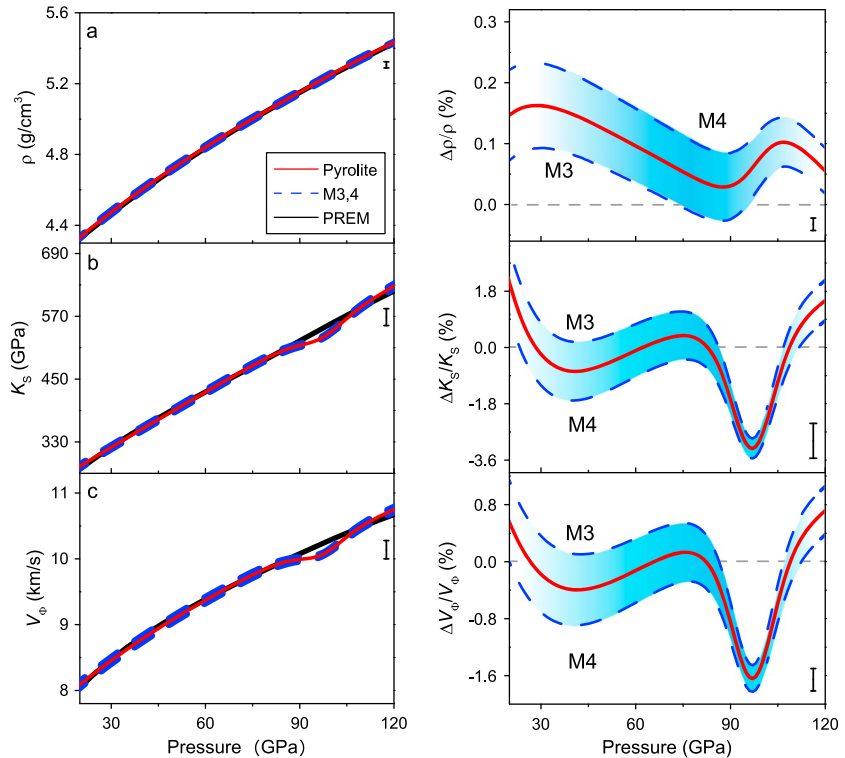
Figure 9. Modeled density (ρ), isothermal bulk modulus (K_T), and bulk sound velocity (V_Φ) of the lower mantle with a variation in the amount of CaSiO$_3$ perovskite. Black line: PREM [*Dziewonski and Anderson*, 1981]; red line: lower mantle with a pyrolitic composition; and blue dashed lines: Models M3 and M4. Both M3 and M4 assume that the volume ratio between bridgmanite and ferropericlase is the same as the pyrolitic mantle composition. M3 has a CaSiO$_3$ perovskite content of 0%, whereas M4 has a greater CaSiO$_3$ perovskite content of 16%.
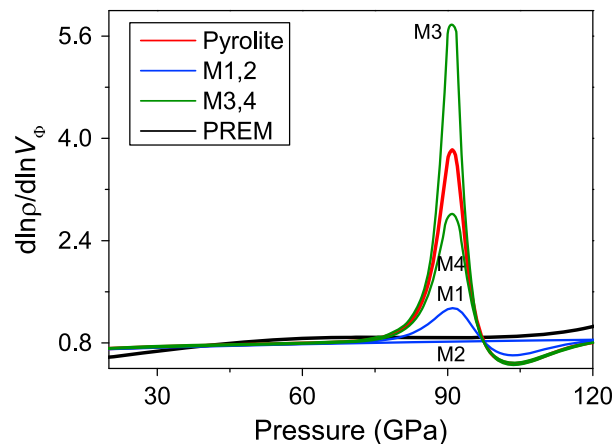
Figure 10. $d\ln\rho/d\ln V_\Phi$ of the lower mantle with pyrolitic and chondritic models. Black line: PREM [*Dziewonski and Anderson*, 1981]; red line: lower mantle with a pyrolitic composition; and green lines: chondritic models M1 and M2 assuming that $CaSiO_3$ perovskite is 8%, the same as that of a pyrolitic mantle composition. M1 has an Mg/Si ratio of 1 with 85% bridgmanite, 7% ferropericlase, and 8% $CaSiO_3$ perovskite, whereas M2 is depleted of ferropericlase with 92% bridgmanite and 8% $CaSiO_3$ perovskite; blue lines: Models M3 and M4. Both M3 and M4 assume that the volume ratio between bridgmanite and ferropericlase is the same as the pyrolitic mantle composition. M3 has a $CaSiO_3$ perovskite content of 0%, whereas M4 has a greater $CaSiO_3$ perovskite content of 16%.

in both pyrolitic and chondritic mantle compositions and examined how the variation of $CaSiO_3$ perovskite content affects the lower mantle $R_{\rho/\Phi}$ profile (Figure 10).

In the seismic PREM, $R_{\rho/\Phi}$ is ~0.6 at the top of the lower mantle at pressures of 24 GPa and continuously increases with pressure to 1 at 120 GPa (~2600 km depth) [*Dziewonski and Anderson*, 1981]. $R_{\rho/\Phi}$ in all of our models has a value of ~0.72, which is slightly greater than that of PREM at 24 GPa, and weakly increases with pressure up to 75 GPa (~2200 km depth) (Figure 10). The difference in $R_{\rho/\Phi}$ between our models in various compositions and PREM is within ±0.1 at less than 75 GPa. Varying the lower mantle composition, particularly the Mg/Si ratio, thus has a negligible effect on $R_{\rho/\Phi}$ between 24 and 75 GPa (Figure 10). Between 75 GPa and 120 GPa, $R_{\rho/\Phi}$ in all of our models, except the chondritic model M2,

exhibits a strong fluctuation with pressure because of the spin transition of Fe in ferropericlase (Figure 9). The value of $R_{\rho/\Phi}$ within the spin crossover is about 2 to 5 times greater than that above and below the spin transition [*Watt et al.*, 1976; *Yang et al.*, 2015]. In this case, the variation of $R_{\rho/\Phi}$ with increasing pressure across the spin crossover provides the crucial information on the presence of ferropericlase in the lower mantle. However, the anomalous variation is absent in the seismic 1-D PREM potentially due to the limited spatial resolution over a wide pressure (depth) range, which needs to be further examined in future seismic studies.

7. Conclusions

In summary, we have performed high P-T XRD measurements to determine the thermal EoS parameters of cubic $CaSiO_3$ perovskite using laser-heated DACs and discussed the potential cause for the conflicting results in literature. Using the new experimental results together with reevaluation the literature results for the thermal EoS parameters of lower mantle bridgmanite and ferropericlase, we have modeled the ρ, K_S, and V_Φ profiles of the lower mantle. Combining our modeling results for the ρ, K_S, and V_Φ profiles, we conclude that predictions for a pyrolitic composition have seismic properties in better agreement with the PREM than lower mantle with a chondritic composition, which is consistent with recent theoretical modeling results for the shear and compressional wave velocities of the lower mantle [*Wang et al.*, 2015; *Zhang et al.*, 2016]. The upper and lower mantle could thus be chemically homogenous, as a consequence of the whole mantle convection of material circulation.

In addition, our modeling also shows that the ρ and V_Φ profiles of the lower mantle is not sensitive to the variations in the content of $CaSiO_3$ perovskite but mainly controlled by the relative volume ratio of bridgmanite and ferropericlase. Since cubic $CaSiO_3$ perovskite in the lower mantle is expected to exhibit a stronger seismic anisotropy and a lower shear velocity than bridgmanite, future experimental studies for the full-elastic tensor of the cubic $CaSiO_3$ perovskite are needed for critical examination of the role of $CaSiO_3$ perovskite on the seismic profiles of the lower mantle [*Kawai and Tsuchiya*, 2015]. It is worth noting that the composition of the lower mantle in this study is only constrained by the modeled ρ and V_Φ profiles. Future experimental studies which provide direct constraints on V_P and V_S at relevant P-T conditions of the lower mantle are

needed to confirm the modeling results in the study and provide more comprehensive understanding on the composition of the Earth's lower mantle.

References

Anderson, D. L. (1983), Chemical composition of the mantle, *J. Geophys. Res.*, *88*, B41–B52, doi:10.1029/JB088iS01p00B41.

Anderson, D. L. (1989), *Theory of the Earth*, Blackwell Sci., Oxford, U. K.

Andrault, D., N. Bolfan-Casanova, and N. Guignot (2001), Equation of state of lower mantle (Al,Fe)-MgSiO$_3$ perovskite, *Earth Planet. Sci. Lett.*, *193*, 501–508.

Antonangeli, D., J. Siebert, C. M. Aracne, D. L. Farber, A. Bosak, M. Hoesch, M. Krisch, F. J. Ryerson, G. Fiquet, and J. Badro (2011), Spin crossover in ferropericlase at high pressure: A seismologically transparent transition?, *Science*, *331*, 64–67.

Badro, J., G. Fiquet, F. Guyot, J. P. Rueff, V. V. Struzhkin, G. Vanko, and G. Monaco (2003), Iron partitioning in Earth's mantle: Toward a deep lower mantle discontinuity, *Science*, *300*, 789–791.

Ballaran, T. B., A. Kurnosov, K. Glazyrin, D. J. Frost, M. Merlini, M. Hanfland, and R. Caracas (2012), Effect of chemistry on the compressibility of silicate perovskite in the lower mantle, *Earth Planet. Sci. Lett.*, *333*, 181–190.

Brown, J. M., and T. J. Shankland (1981), Thermodynamic parameters in the Earth as determined from seismic profiles, *Geophys. J. R. Astron. Soc.*, *66*, 579–596.

Cammarano, F., and B. Romanowicz (2007), Insights into the nature of the transition zone from physically constrained inversion of long-period seismic data, *Proc. Natl. Acad. Sci. U.S.A.*, *104*, 9139–9144.

Caracas, R., and R. M. Wentzcovitch (2006), Theoretical determination of the structures of CaSiO$_3$ perovskites, *Acta Crystallogr., Sect. B*, *62*, 1025–1030.

Catalli, K., S. H. Shim, V. B. Prakapenka, J. Zhao, and W. Sturhahn (2010), X-ray diffraction and Mossbauer spectroscopy of Fe^{3+}-bearing Mg-silicate post-perovskite at 128–138 GPa, *Am. Mineral.*, *95*, 418–421.

Catalli, K., S. H. Shim, P. Dera, V. B. Prakapenka, J. Y. Zhao, W. Sturhahn, P. Chow, Y. M. Xiao, H. Cynn, and W. J. Evans (2011), Effects of the Fe^{3+} spin transition on the properties of aluminous perovskite—New insights for lower-mantle seismic heterogeneities, *Earth Planet. Sci. Lett.*, *310*, 293–302.

Chen, B., J. M. Jackson, W. Sturhahn, D. Z. Zhang, J. Y. Zhao, J. K. Wicks, and C. A. Murphy (2012), Spin crossover equation of state and sound velocities of (Mg$_{0.65}$Fe$_{0.35}$)O ferropericlase to 140 GPa, *J. Geophys. Res.*, *117*, B08208, doi:10.1029/2012JB009162.

Chizmeshya, A. V. G., G. H. Wolf, and P. F. McMillan (1996), First-principles calculation of the equation-of-state, stability, and polar optic modes of CaSiO$_3$ perovskite, *Geophys. Res. Lett.*, *23*, 2725–2728.

Cottaar, S., T. Heister, I. Rose, and C. Unterborn (2014), BurnMan: A lower mantle mineral physics toolkit, *Geochem. Geophys. Geosyst.*, *15*, 1164–1179, doi:10.1002/2013GC005122.

Crowhurst, J. C., J. M. Brown, A. F. Goncharov, and S. D. Jacobsen (2008), Elasticity of (Mg,Fe)O through the spin transition of iron in the lower mantle, *Science*, *319*, 451–453.

Dewaele, A., P. Loubeyre, and M. Mezouar (2004), Equations of state of six metals above 94 GPa, *Phys. Rev. B*, *70*, 094112, doi:10.1103/Physrevb.70.094112.

Dobson, D. P., and J. P. Brodholt (2005), Subducted banded iron formations as a source of ultralow-velocity zones at the core-mantle boundary, *Nature*, *434*, 371–374.

Dorfman, S. M., Y. Meng, V. B. Prakapenka, and T. S. Duffy (2013), Effects of Fe-enrichment on the equation of state and stability of (Mg,Fe)SiO$_3$ perovskite, *Earth Planet. Sci. Lett.*, *361*, 249–257.

Dorogokupets, P. I., and A. Dewaele (2007), Equations of state of MgO, au, pt, NaCl-B1, and NaCl-B2: Internally consistent high-temperature pressure scales, *High Pressure Res.*, *27*(4), 431–446.

Duffy, T. S., and D. L. Anderson (1989), Seismic velocities in mantle minerals and the mineralogy of the upper mantle, *J. Geophys. Res.*, *94*, 1895–1912.

Dziewonski, A. M., and D. L. Anderson (1981), Preliminary reference Earth model, *Phys. Earth Planet. Inter.*, *25*, 297–356.

Fei, Y. W., A. Ricolleau, M. Frank, K. Mibe, G. Y. Shen, and V. Prakapenka (2007a), Toward an internally consistent pressure scale, *Proc. Natl. Acad. Sci. U.S.A.*, *104*, 9182–9186.

Fei, Y. W., L. Zhang, A. Corgne, H. Watson, A. Ricolleau, Y. Meng, and V. Prakapenka (2007b), Spin transition and equations of state of (Mg, Fe)O solid solutions, *Geophys. Res. Lett.*, *34*, L17307, doi:10.1029/2007GL030712.

Fiquet, G., A. Dewaele, D. Andrault, M. Kunz, and T. Le Bihan (2000), Thermoelastic properties and crystal structure of MgSiO$_3$ perovskite at lower mantle pressure and temperature conditions, *Geophys. Res. Lett.*, *27*, 21–24.

Funamori, N., R. Jeanloz, N. Miyajima, and K. Fujino (2000), Mineral assemblages of basalt in the lower mantle, *J. Geophys. Res.*, *105*, 26,037–26,043.

Garnero, E. J., and A. K. McNamara (2008), Structure and dynamics of Earth's lower mantle, *Science*, *320*, 626–628.

Glazyrin, K., T. B. Ballaran, D. J. Frost, C. McCammon, A. Kantor, M. Merlini, M. Hanfland, and L. Dubrovinsky (2014), Magnesium silicate perovskite and effect of iron oxidation state on its bulk sound velocity at the conditions of the lower mantle, *Earth Planet. Sci. Lett.*, *393*, 182–186.

Hama, J., and K. Suito (1998), High-temperature equation of state of CaSiO$_3$ perovskite and its implications for the lower mantle, *Phys. Earth Planet. Inter.*, *105*, 33–46.

Hart, S. R., and A. Zindler (1986), In search of a bulk-Earth composition, *Chem. Geol.*, *57*, 247–267.

Hirose, K., Y. W. Fei, Y. Z. Ma, and H. K. Mao (1999), The fate of subducted basaltic crust in the Earth's lower mantle, *Nature*, *397*, 53–56.

Hofmann, A. W. (1988), Chemical differentiation of the Earth: The relationship between mantle, continental crust, and oceanic crust, *Earth Planet. Sci. Lett.*, *90*, 297–314.

Hsu, H., P. Blaha, M. Cococcioni, and R. M. Wentzcovitch (2011), Spin-state crossover and hyperfine interactions of ferric iron in MgSiO$_3$ perovskite, *Phys. Rev. Lett.*, *106*, 118501, doi:10.1103/Physrevlett.106.118501.

Hsu, H., Y. G. G. Yu, and R. M. Wentzcovitch (2012), Spin crossover of iron in aluminous MgSiO3 perovskite and post-perovskite, *Earth Planet. Sci. Lett.*, *359*, 34–39.

Irifune, T., T. Shinmei, C. A. McCammon, N. Miyajima, D. C. Rubie, and D. J. Frost (2010), Iron partitioning and density changes of pyrolite in Earth's lower mantle, *Science*, *327*, 193–195.

Ishii, M., and J. Tromp (2004), Constraining large-scale mantle heterogeneity using mantle and inner-core sensitive normal modes, *Phys. Earth Planet. Inter.*, *146*, 113–124.

Jackson, I., and S. M. Rigden (1996), Analysis of P-V-T data: Constraints on the thermoelastic properties of high-pressure minerals, *Phys. Earth Planet. Inter.*, *96*, 85–112.

Jacobsen, S. D., H. J. Reichmann, H. A. Spetzler, S. J. Mackwell, J. R. Smyth, R. J. Angel, and C. A. McCammon (2002), Structure and elasticity of single-crystal (Mg,Fe)O and a new method of generating shear waves for gigahertz ultrasonic interferometry, *J. Geophys. Res.*, *107*(B2), 2037, doi:10.1029/2001JB000490.

Jacobsen, S. D., C. M. Holl, K. A. Adams, R. A. Fischer, E. S. Martin, C. R. Bina, J. F. Lin, V. B. Prakapenka, A. Kubo, and P. Dera (2008), Compression of single-crystal magnesium oxide to 118 GPa and a ruby pressure gauge for helium pressure media, *Am. Mineral.*, *93*, 1823–1828.

Javoy, M. (1995), The integral enstatite chondrite model of the Earth, *Geophys. Res. Lett.*, *22*, 2219–2222.

Jung, D. Y., and A. R. Oganov (2005), Ab initio study of the high-pressure behavior of CaSiO$_3$ perovskite, *Phys. Chem. Miner.*, *32*, 146–153.

Kaminski, E., and M. Javoy (2013), A two-stage scenario for the formation of the Earth's mantle and core, *Earth Planet. Sci. Lett.*, *365*, 97–107.

Karki, B. B., and J. Crain (1998), First-principles determination of elastic properties of CaSiO$_3$ perovskite at lower mantle pressures, *Geophys. Res. Lett.*, *25*, 2741–2744.

Kawai, K., and T. Tsuchiya (2014), P-V-T equation of state of cubic CaSiO$_3$ perovskite from first-principles computation, *J. Geophys. Res. Solid Earth*, *119*, 2801–2809, doi:10.1002/2013JB010905.

Kawai, K., and T. Tsuchiya (2015), Small shear modulus of cubic CaSiO$_3$ perovskite, *Geophys. Res. Lett.*, *42*, 2718–2726, doi:10.1002/2015GL063446.

Kirby, S. H., S. Stein, E. A. Okal, and D. C. Rubie (1996), Metastable mantle phase transformations and deep earthquakes in subducting oceanic lithosphere, *Rev. Geophys.*, *34*, 261–306.

Komabayashi, T., K. Hirose, Y. Nagaya, E. Sugimura, and Y. Ohishi (2010), High-temperature compression of ferropericlase and the effect of temperature on iron spin transition, *Earth Planet. Sci. Lett.*, *297*, 691–699.

Kurashina, T., K. Hirose, S. Ono, N. Sata, and Y. Ohishi (2004), Phase transition in Al-bearing CaSiO$_3$ perovskite: Implications for seismic discontinuities in the lower mantle, *Phys. Earth Planet. Int.*, *145*(1–4), 67–74.

Lay, T., Q. Williams, and E. J. Garnero (1998), The core-mantle boundary layer and deep Earth dynamics, *Nature*, *392*, 461–468.

Lee, C. T. A., P. Luffi, T. Hoink, J. Li, R. Dasgupta, and J. Hernlund (2010), Upside-down differentiation and generation of a 'primordial' lower mantle, *Nature*, *463*, 930–933, doi:10.1038/nature08824.

Li, B., and R. C. Liebermann (2007), Indoor seismology by probing the Earth's interior by using sound velocity measurements at high pressures and temperatures, *Proc. Natl. Acad. Sci. U.S.A.*, *104*, 9145–9150.

Li, J., V. V. Struzhkin, H. K. Mao, J. F. Shu, R. J. Hemley, Y. W. Fei, B. Mysen, P. Dera, V. Prakapenka, and G. Y. Shen (2004), Electronic spin state of iron in lower mantle perovskite, *Proc. Natl. Acad. Sci. U.S.A.*, *101*, 14,027–14,030.

Lin, J. F., V. V. Struzhkin, S. D. Jacobsen, M. Y. Hu, P. Chow, J. Kung, H. Z. Liu, H. K. Mao, and R. J. Hemley (2005), Spin transition of iron in magnesiowustite in the Earth's lower mantle, *Nature*, *436*, 377–380.

Lin, J. F., E. E. Alp, Z. Mao, T. Inoue, C. McCammon, Y. M. Xia, P. Chow, and J. Y. Zhao (2012), Electronic spin states of ferric and ferrous iron in the lower-mantle silicate perovskite, *Am. Mineral.*, *97*, 592–597.

Lin, J. F., S. Speziale, Z. Mao, and H. Marquardt (2013), Effects of the electronic spin transitions of iron in lower-mantle minerals: Implications to deep-mantle geophysics and geochemistry, *Rev. Geophys.*, *51*, 244–275, doi:10.1002/rog.20010.

Lundin, S., K. Catalli, J. Santillan, S. H. Shim, V. B. Prakapenka, M. Kunz, and Y. Meng (2008), Effect of Fe on the equation of state of mantle silicate perovskite over 1 Mbar, *Phys. Earth Planet. Inter.*, *168*, 97–102.

Magyari-Kope, B., L. Vitos, G. Grimvall, B. Johansson, and J. Kollar (2002), Low-temperature crystal structure of CaSiO$_3$ perovskite: An ab initio total energy study, *Phys. Rev. B*, *65*, 193107, doi:10.1103/PhysRevB.65.193107.

Mao, Z., J. F. Lin, J. Liu, and V. B. Prakapenka (2011a), Thermal equation of state of lower-mantle ferropericlase across the spin crossover, *Geophys. Res. Lett.*, *38*, L23308, doi:10.1029/2011GL049915.

Mao, Z., J. F. Lin, H. P. Scott, H. C. Watson, V. B. Prakapenka, Y. Xiao, P. Chow, and C. McCammon (2011b), Iron-rich perovskite in the Earth's lower mantle, *Earth Planet. Sci. Lett.*, *309*, 179–184.

Mao, Z., et al. (2014), (Fe, Al)-bearing post-perovskite in the Earth's lower mantle, *Earth Planet. Sci. Lett.*, *403*, 157–165.

Mao, Z., J. F. Lin, J. Yang, T. Inoue, and V. B. Prakapenka (2015), Effects of the Fe^{3+} spin transition on the equation of state of bridgmanite, *Geophys. Res. Lett.*, *42*, 4335–4342, doi:10.1002/2015GL064400.

Marquardt, H., S. Speziale, H. J. Reichmann, D. J. Frost, and F. R. Schilling (2009a), Single-crystal elasticity of (Mg$_{0.9}$Fe$_{0.1}$)O to 81 GPa, *Earth Planet. Sci. Lett.*, *287*, 345–352.

Marquardt, H., S. Speziale, H. J. Reichmann, D. J. Frost, F. R. Schilling, and E. J. Garnero (2009b), Elastic shear anisotropy of ferropericlase in Earth's lower mantle, *Science*, *324*, 224–226.

Matas, J., J. Bass, Y. Ricard, E. Mattern, and M. S. I. Bukowinski (2007), On the bulk composition of the lower mantle: Predictions and limitations from generalized inversion of radial seismic profiles, *Geophys. J. Int.*, *170*, 764–780.

McCammon, C., I. Kantor, O. Narygina, J. Rouquette, U. Ponkratz, I. Sergueev, M. Mezouar, V. Prakapenka, and L. Dubrovinsky (2008), Stable intermediate-spin ferrous iron in lower-mantle perovskite, *Nat. Geosci.*, *1*, 684–687.

Mcdonough, W. F., and S. S. Sun (1995), The composition of the Earth, *Chem. Geol.*, *120*, 223–253.

Morgan, J. W., and E. Anders (1980), Chemical composition of Earth, Venus, and Mercury, *Proc. Natl. Acad. Sci. U.S.A.*, *77*(12), 6973–6977, doi:10.1073/pnas.77.12.6973.

Murakami, M., S. V. Sinogeikin, H. Hellwig, J. D. Bass, and J. Li (2007), Sound velocity of MgSiO$_3$ perovskite to Mbar pressure, *Earth Planet. Sci. Lett.*, *256*, 47–54.

Murakami, M., Y. Ohishi, N. Hirao, and K. Hirose (2012), A perovskitic lower mantle inferred from high-pressure, high-temperature sound velocity data, *Nature*, *485*(7396), 90–94.

Narygina, O. V., I. Y. Kantor, C. A. McCammon, and L. S. Dubrovinsky (2010), Electronic state of Fe^{2+} in (Mg,Fe)(Si,Al)O$_3$ perovskite and (Mg,Fe)SiO$_3$ majorite at pressures up to 81 GPa and temperatures up to 800 K, *Phys. Chem. Miner.*, *37*, 407–415.

Ni, S., E. Tan, M. Gurnis, and D. Helmberger (2002), Sharp sides to the African superplume, *Science*, *296*, 1850–1852.

Nishio-Hamane, D., Y. Seto, K. Fujino, and T. Nagai (2008), Effect of FeAlO$_3$ incorporation into MgSiO$_3$ on the bulk modulus of perovskite, *Phys. Earth Planet. Inter.*, *166*, 219–225.

Noguchi, M., T. Komabayashi, K. Hirose, and Y. Ohishi (2013), High-temperature compression experiments of CaSiO$_3$ perovskite to lowermost mantle conditions and its thermal equation of state, *Phys. Chem. Miner.*, *40*, 81–91.

Ono, S., Y. Ohishi, and K. Mibe (2004), Phase transition of Ca-perovskite and stability of Al-bearing Mg-perovskite in the lower mantle, *Am. Mineral.*, *89*, 1480–1485.

Palme, H., and A. Jones (2003), Solar system abundances of the elements, in *Treatise on Geochemistry*, edited by H. Holland and K. K. Turekian, pp. 1–38 , Elsevier, New York.

Panero, W. R., S. Akber-Knutson, and L. Stixrude (2006), Al$_2$O$_3$ incorporation in MgSiO$_3$ perovskite and ilmenite, *Earth Planet. Sci. Lett.*, *252*, 152–161.

Perrillat, J. P., A. Ricolleau, I. Daniel, G. Fiquet, M. Mezouar, N. Guignot, and H. Cardon (2006), Phase transformations of subducted basaltic crust in the upmost lower mantle, *Phys. Earth Planet. Inter.*, *157*, 139–149.

Prakapenka, V. B., A. Kubo, A. Kuznetsov, A. Laskin, O. Shkurikhin, P. Dera, M. L. Rivers, and S. R. Sutton (2008), Advanced flat top laser heating system for high pressure research at GSECARS: Application to the melting behavior of germanium, *High Pressure Res.*, *28*, 225–235.

Ricolleau, A., et al. (2009), Density profile of pyrolite under the lower mantle conditions, *Geophys. Res. Lett.*, *36*, L06302, doi:10.1029/2008GL036759.

Ringwood, A. E. (1975), *Composition and Petrology of the Earth's Mantle*, xvi, 618 pp., McGraw-Hill, New York.

Romanowicz, B. (2001), Can we resolve 3D density heterogeneity in the lower mantle?, *Geophys. Res. Lett.*, *28*, 1107–1110.

Saikia, A., T. B. Ballaran, and D. J. Frost (2009), The effect of Fe and Al substitution on the compressibility of $MgSiO_3$-perovskite determined through single-crystal X-ray diffraction, *Phys. Earth Planet. Inter.*, *173*, 153–161.

Sherman, D. M. (1993), Equation of state, elastic properties, and stability of $CaSiO_3$ perovskite: First principles (periodic Hartree-Fock) results, *J. Geophys. Res.*, *98*, 19,795–19,805.

Shim, S. H., T. S. Duffy, and G. Y. Shen (2000), The stability and P-V-T equation of state of $CaSiO_3$ perovskite in the Earth's lower mantle, *J. Geophys. Res.*, *105*, 25,955–25,968.

Shim, S.-H., R. Jeanloz, and T. S. Duffy (2002), Tetragonal structure of $CaSiO_3$ perovskite above 20 GPa, *Geophys. Res. Lett.*, *29*(24), 2166, doi:10.1029/2002GL016148.

Simmons, N. A., A. M. Forte, and S. P. Grand (2009), Joint seismic, geodynamic and mineral physical constraints on three-dimensional mantle heterogeneity: Implications for the relative importance of thermal versus compositional heterogeneity, *Geophys. J. Int.*, *177*, 1284–1304.

Speziale, S., C. S. Zha, T. S. Duffy, R. J. Hemley, and H. K. Mao (2001), Quasi-hydrostatic compression of magnesium oxide to 52 GPa: Implications for the pressure-volume-temperature equation of state, *J. Geophys. Res.*, *106*, 515–528.

Speziale, S., V. E. Lee, S. M. Clark, J. F. Lin, M. P. Pasternak, and R. Jeanloz (2007), Effects of Fe spin transition on the elasticity of (Mg, Fe) O magnesiowüstites and implications for the seismological properties of the Earth's lower mantle, *J. Geophys. Res.*, *112*, B10212, doi:10.1029/2006JB004730.

Stixrude, L., C. Lithgow-Bertelloni, B. Kiefer, and P. Fumagalli (2007), Phase stability and shear softening in $CaSiO_3$ perovskite at high pressure, *Phys. Rev. B*, *75*, 024108, doi:10.1103/PhysRevB.75.024108.

Tamai, H., and T. Yagi (1989), High-pressure and high-temperature phase-relations in $CaSiO_3$ and $CaMgSi_2O_6$ and elasticity of perovskite-type $CaSiO_3$, *Phys. Earth Planet. Inter.*, *54*, 370–377.

Tange, Y., Y. Kuwayama, T. Irifune, K. Funakoshi, and Y. Ohishi (2012), P-V-T equation of state of $MgSiO_3$ perovskite based on the MgO pressure scale: A comprehensive reference for mineralogy of the lower mantle, *J. Geophys. Res.*, *117*, B06201, doi:10.1029/2011JB008988.

Trampert, J., F. Deschamps, J. Resovsky, and D. Yuen (2004), Probabilistic tomography maps chemical heterogeneities throughout the lower mantle, *Science*, *306*, 853–856.

Tsuchiya, T. (2003), First-principles prediction of the P-V-T equation of state of gold and the 660-km discontinuity in Earth's mantle, *J. Geophys. Res.*, *108*(B10), 2462, doi:10.1029/2003JB002446.

Tsuchiya, T., and X. L. Wang (2013), Ab initio investigation on the high-temperature thermodynamic properties of Fe^{3+}-bearing $MgSiO_3$ perovskite, *J. Geophys. Res. Solid Earth*, *118*, 83–91, doi:10.1029/2012JB009696.

Wang, X. L., T. Tsuchiya, and A. Hase (2015), Computational support for a pyrolitic lower mantle containing ferric iron, *Nat. Geosci.*, *8*, 556–559.

Wang, Y., and L. Wen (2007), Geometry and P and S velocity structure of the "African Anomaly", *J. Geophys. Res.*, *112*, B05313, doi:10.1029/2006JB004483.

Wang, Y. B., D. J. Weidner, and F. Guyot (1996), Thermal equation of state of $CaSiO_3$ perovskite, *J. Geophys. Res.*, *101*, 661–672.

Watt, J. P., G. F. Davies, and R. J. Oconnell (1976), Elastic properties of composite-materials, *Rev. Geophys.*, *14*, 541–563.

Wentzcovitch, R. M., N. L. Ross, and G. D. Price (1995), Ab-initio study of $MgSiO_3$ and $CaSiO_3$ perovskites at lower-mantle pressures, *Phys. Earth Planet. Inter.*, *90*, 101–112.

Wentzcovitch, R. M., J. F. Justo, Z. Wu, C. R. S. da Silva, D. A. Yuen, and D. Kohlstedt (2009), Anomalous compressibility of ferropericlase throughout the iron spin cross-over, *Proc. Natl. Acad. Sci. U.S.A.*, *106*, 8447–8452.

Williams, Q., and E. Knittle (2005), The uncertain major element bulk composition of Earth's mantle, in *Earth's Deep Mantle: Structure, Composition and Evolution*, edited by R. D. Van der Hilst et al., pp. 189–202, AGU, Washington, D. C.

Wolf, A. S., J. M. Jackson, P. Dera, and V. Prakapenka (2015), The thermal equation of state of (Mg, Fe)SiO_3 bridgmanite (perovskite) and implications for lower mantle structures, *J. Geophys. Res. Solid Earth*, *120*, 7460–7489, doi:10.1002/2015JB012108.

Wolf, G. H., and R. Jeanloz (1985), Lattice-dynamics and structural distortions of $MgSiO_3$ and $CaSiO_3$ perovskites, *Geophys. Res. Lett.*, *12*, 413–416.

Yang, J., X. Y. Tong, J. F. Lin, T. Okuchi, and N. Tomioka (2015), Elasticity of ferropericlase across the spin crossover in the Earth's lower mantle, *Sci. Rep.*, *5*, 17188, doi:10.1038/Srep17188.

Zhang, S., S. Cottaar, T. Liu, S. Stackhouse, and B. Militzer (2016), High-pressure, temperature elasticity of Fe- and Al-bearing $MgSiO_3$: Implications for the Earth's lower mantle, *Earth Planet. Sci. Lett.*, *434*, 264–273.

Zhang, Y. G., D. P. Zhao, M. Matsui, and G. J. Guo (2006), Equations of state of $CaSiO_3$ Perovskite: A molecular dynamics study, *Phys. Chem. Miner.*, *33*, 126–137.